ゲスト分子で構造制御された層状ホスト化合物を用いるインテリジェント触媒の創製

(課題番号 09650972)

平成９年度～平成１０年度科学研究費補助金
(基盤研究（C）)
研究成果報告書

平成１１年３月

研究代表者　島津　省吾
(千葉大学工学部助教授)

研究組織

研究代表者：　島　津　省　吾　　（千葉大学工学部助教授）

研究経費

平成9年度	3、200千円
平成10年度	400千円
計	3、600千円

研究発表

学会誌等

(1)島津省吾，ソフト化学的手法によるイオン交換体の化学修飾と分子認識触媒への応用、*日本イオン交換学会誌*、8(1)、2-16 (1997).

(2)T. Sento, S. Shimazu, N. Ichikuni, and T. Uematsu, New Clay-Supported Chiral Rhodium Complexes: Interlayer Modification with Tuning Guests and Asymmetric Hydrogenation, *Chem. Lett.*, 1191-1192(1998).

(3)T. Sento, S. Shimazu, N. Ichikuni, and T. Uematsu, Asymmetric Hydrogenation of Itaconates by Hectorite-Intercalated Rh-DIOP Complex, *J. Mol. Catalysis A: Chemical*, 137, 263-267(1999).

(4)S. Shimazu, T. Sento, N. Ichikuni, and T. Uematsu, Selective Hydrogenation of ketones by Multi-Modified Clay Catalysts, *Bull. Chem. Soc. Jpn* (1999) (投稿予定).

口頭発表

(5)S. Shimazu, K. Uematsu, N. Ichikuni, and T. Uematsu: Selective Hydrogenation Catalyzed by Rhodium(I)-Chitosan Complex Supported on Smectite, *International Symposium on Zeolites and Microporous Crystals*, Tokyo, P.220, August 27, 1997.

(6)仙頭 準、島津省吾、一國伸之、上松敬禧：アルキルアンモニウムで構造制御したヘクトライト層間固定化Rh錯体による不斉水素化反応、*平成9年度触媒研究発表会*、*触媒学会（信州大学）*、講演番号3F20、1997年9月19日.

(7)島津省吾、狩山雅洋、一國伸之、上松敬禧：アニオン交換性層状化合物の不斉修飾と分子認識能、*第13回日本イオン交換研究発表会*、日本イオン交換学会（山梨大学）、P-30、1997年10月2日.

(8)仙頭 準、一國伸之、島津省吾、上松敬禧：アルキルアンモニウムで構造制御した層間固定化Rh錯体による不斉水素化反応、*第13回日本イオン交換研究発表会*、日本イオン交換学会（山梨大学）、P-31、1997年10月2日.

(9)粂野正樹、一國伸之、島津省吾、上松敬禧：Rh(I)-アミロース錯体の粘土鉱物層間への固定化と不斉水素化触媒反応、*第13回日本イオン交換研究発表会*、日本イオン交換学会（山梨大学）、P-33、1997年10月2日.

(10)田崎 賢、一國伸之、島津省吾、上松敬禧：層間固定化ロジウム錯体による不飽和カルボニル化合物の不斉水素化反応、*第13回日本イオン交換研究発表会*、日本イオン交換

学会（山梨大学）、P-34、1997年10月2日.

(11)桑原紀子、一國伸之、島津省吾、上松敬禧：ヘクトライト層間固定化錯体による不飽和エステルの不斉水素化反応－担持量による層間隔制御と不斉選択性への影響－、*第13回日本イオン交換研究発表会*、日本イオン交換学会（山梨大学）、3-I-6、1997年10月3日.

(12)島津省吾：Chiral Modification of Layer Compounds with Organic Anions and Application to Molecular Recognition, *The 5th International Symposium on Separation Chemistry*、科技庁無機材質研究所（つくば市）、講演番号4、1997年10月6日.

(13)仙頭 準、島津省吾、一國伸之、上松敬禧：チューニングゲストで構造制御した層間固定化ロジウム錯体による不斉水素化反応、*シンポジウム「コンセプチュアルアプローチ in 触媒」*、触媒学会（東京大学理学部）、講演番号2、1997年12月12日.

(14)島津省吾，仙頭準，一國伸之，上松敬禧：チューニングゲストで構造制御されたヘクトライト層間固定化Rh錯体による不斉水素化反応，*日本化学会第74春季年会（同志社大学）*，講演番号1H117，1998年3月27日.

(15)島津省吾，高山日出樹，柏崎史，一國伸之，上松敬禧：ボタラッカイト型層状化合物の不斉修飾と分子認識取込反応，*日本化学会第74春季年会（同志社大学）*，講演番号1PA004，1998年3月27日.

(16)島津省吾，岩村響，植松克也，一國伸之，上松敬禧：粘土鉱物層間固定化ロジウム－キトサン錯体触媒による選択的部分水素化反応，*日本化学会第74春季年会（同志社大学）*，講演番号1PB124，1998年3月27日.

(17)S. Shimazu, Preparation of Clay-Supported Complexes and Application to Shape Selective Catalyses, *Seminar (Oxford University)*, Oxford, July 15, 1998.

(18)S. Shimazu, K. Uematsu, N. Ichikuni, and T. Uematsu: Selective Hydrogenation Catalyzed by Rhodium(I)-Sugar Complex Supported on Smectite, *9th International Symposium on Relations Between Homogeneous and Heterogeneous Catalysis (Southampton), Abstracts,* P. 52, July 20, 1998.

(19)島津省吾，仙頭準，一國伸之，上松敬禧：チューニングゲストで立体構造制御された層間固定化Rh錯体の反応性、*日本化学会第75秋季年会（松山市）*，講演番号3B603，1998年9月17日.

(20)島津省吾，近藤広行，一國伸之，上松敬禧：ニッケルー亜鉛酢酸塩層状化合物の不斉修飾とその分子認識性、*日本化学会第75秋季年会（松山市）*，講演番号4B509，1998年9月18日.

(21)島津省吾，近藤広行，一國伸之，上松敬禧：不斉有機アニオンによるNi-Zn酢酸塩の化学修飾とその分子認識性，*第14回日本イオン交換研究発表会（佐賀市）*，講演番号2-02，1998年10月29日.

(22)島津省吾、桑原紀子、一國伸之、上松敬禧，構造制御されたスメクタイト固定化Rh-BPPFA錯体による不斉水素化反応，*シンポジウム「コンセプチュアルアプローチ in 触媒」*、触媒学会（早稲田大学国際会議場）、講演番号1、1998年12月11日.

(23)島津省吾、仙頭　準、一國伸之、上松敬禧、構造制御されたスメクタイト固定化Rh-

DIOP 錯体の触媒挙動、*シンポジウム「コンセプチュアルアプローチ in 触媒」*、触媒学会（早稲田大学国際会議場）、講演番号２、1998 年 12 月 11 日.

(24)Shogo Shimazu、Structural Modification of Smectites with Tuning Guests and Catalysis for Molecular Recognition Reactions, *The 14th International Symposium on Separation Chemistry,* 無機材質研究所、No. 3、Jan. 18, 1999.

(25)島津省吾、仙頭準、一國伸之、上松敬禧：アルキルアンモニウム修飾した粘土層間固定化 Rh-ホスフィン錯体による選択的水素化反応、*日本化学会第 76 春季年会（神奈川大学）*，講演番号 4F517、1999 年 3 月 31 日.

(26)島津省吾、鈴木雅之、一國伸之、上松敬禧：層間固定化 Rh-BINAP 錯体によるケトンの不斉水素化－アミンの添加効果－、*日本化学会第 76 春季年会（神奈川大学）*，講演番号 4F518、1999 年 3 月 31 日.

出版物

(27)築部浩　編、　島津省吾　分筆、*分子認識化学*、　三共出版　1997 年 4 月.

研究成果

目次

本文

１．　概要

本研究は、イオン交換性の層状スメクタイト系粘土鉱物をホストとして用い、これらの層内表面を構造チューニングゲスト、不斉配位子および遷移金属錯体で化学修飾して種々の層間サイズを有する新規な層間固定化錯体触媒を創製した。特筆すべき点として、（１）ｱﾙｷﾙｱﾝﾓﾆｳﾑ(C_nN^+)修飾層状粘土鉱物への Rh-ﾎｽﾌｨﾝ錯体のｲﾝﾀｰｶﾚｰｼｮﾝと様々な層間距離を持つ多重修飾層間固定化錯体(MMS)の合成、(2)ホストの層電荷密度を変えることによるゲスト分子の立体化学制御、(3)MMS を触媒とする不斉など高度な分子認識触媒機能についての評価、（４）MMS の層間サイズおよび層間ゲストの立体構造変化が及ぼす触媒挙動の明確化等を行った。すなわち、構造チューニングゲスト修飾という斬新な概念を導入して、層状構造を安定に保持した層間固定化錯体触媒を創製した。具体的には、用いた C_nN^+は１級（$C_nH_{2n+2}NH_3^+$、$1°C_n$）および４級ｱﾝﾓﾆｳﾑ（$(C_nH_{2n+2})_2(CH_3)_2NH_3^+$、$4°C_n$）で炭素数（$C_n$）を 10、14、18 と変えたところ、$1°C_n$でクリアランススペース(CS)=0.37～1.07nm（ΔCS=0.7nm）、$4°C_n$で CS=1.93～2.88nm（ΔCS=0.95nm）の範囲で層間サイズ制御することが出来た。この結果、触媒活性およびその分子認識性は構造チューニングゲストのサイズと配向性に強く依存することを見出した。すなわち、α-ﾋﾟﾈﾝの不斉水素化を行ったところ、低電荷密度のヘクトライト(NaHT)をホストに用いた Rh-DIOP/C_nN^+/NaHT(CS=2.46～2.78nm)では、収率が 1.3～7.3%で選択性は 50～70%e.e.であったが、約 3 倍の電荷密度を有するテニオライト(LiTN)をホストに用いた Rh-DIOP/C_nN^+/LiTN(CS=1.93～2.88nm)では、収率は 99.8%、選択性は 92%e.e.にまで向上した。さらに、高圧条件下(30 気圧)において均一系錯体は活性および選択性が著しく低下するのに対し、MMS 触媒は著しく高い値を維持し、安定な触媒であることを見出した。さらに、ケトンの水素化においても活性を示した。

以上の成果より、結晶性粘土鉱物ﾎｽﾄの層間を構造ﾁｭｰﾆﾝｸﾞｹﾞｽﾄで立体制御すると、触媒活性および不斉選択性を向上させることができた。さらに、他のﾌﾟﾛｷﾗﾙな化合物の不斉水素化反応に展開できると思われる。当初の目的の大部分は達成できたが、同目的の一つである「ﾍｸﾄﾗｲﾄ層間へのﾌｫﾄｸﾛﾐｯｸ化合物のｲﾝﾀｰｶﾚｰｼｮﾝと光化学反応による層構造変化」については、同反応のみではホスト構造を変動させる条件を見出すには至らなかった。

２．　序論

結晶性層状化合物の層空間は触媒反応における分子認識場として非常に重要である。我々は膨潤性に優れたスメクタイト系粘土鉱物の層間に、独自の方法で金属錯体をインターカレートさせた層間固定化金属錯体（Rh-不斉ホスフィン）を合成し、分子認識触媒としての機能を調べた結果、以下の層間化合物に特徴的な触媒挙動を見いだした。すなわち、(1)イタコン酸エステルの不斉水素化触媒反応に対してエステル基のサイズに依存して著しい選択性変化(64-88%e.e.)が見られたが、均一系錯体ではサイズ依存性が見られない（60%e.e.以下）。(2)反応溶媒に対する粘土ホストの膨潤度と不斉選択性の間に相関性を見いだし、膨潤度の小さい溶媒で選択性が著しく増加した。これらの結果は、

均一系錯体のみでは観測されず明らかに粘土ホスト構造が不斉選択性に影響を与えていることを示唆している。他に(3)オレフィンの形状選択水素化、(4)アルキンおよびジエンの部分水素化、位置選択性水素化に高選択性を示すことを見出した。

また、我々は独自の粘土層間修飾法を見いだしている。すなわち、従来のカチオン交換法以外に、層間化学修飾配位子および層間重合配位子への配位子交換法を見出した。よって、金属錯体のインターカレーションでは非水系溶媒が利用できるため、広範囲な錯体を利用した層間固定化触媒が合成可能になった。層間固定化触媒の特徴は、以下の4点が挙げられる：(1)層間を活性種だけでなく、他の構造制御種（チューニングゲスト）も同時に多重修飾可能である。(2)層間距離を厳密に制御することにより、反応活性や選択性を制御できる。(3)比較的大きな高分子（糖、たんぱく質、核酸など）をインターカレートできる。(4)天然に存在する層状結晶の粘土鉱物や安価な金属酸化物塩をホストとして利用することは、化学的・物理的安定性、資源有効利用、経済性から見ても非常に魅力的である。

そこで、本研究では柔軟性のある層構造を種々のチューニングゲストで層間修飾することにより、(1)さまざまな層間距離を持つ固定化錯体を合成し、層間距離が及ぼす触媒反応活性および分子認識性を調べる。(2)光あるいは熱などの外的刺激によりホスト層間距離が変動可能な固定化触媒を創製し、その反応活性および選択性を調べる。ここでは、反応進行中、外的刺激に応答して層構造が瞬時に変化して触媒活性および選択性が変化することから、極めて初歩的であるが自己制御型の触媒、すなわちインテリジェント触媒としての可能性を検討する。

本研究での特色は、第一に、無機層状化合物層間を触媒反応場に利用することにある。第二に、この反応場の空間サイズを任意に変化させて、反応活性および選択性を制御することにある。第三に、反応進行中、外的刺激によりこの層空間を（触媒反応速度に比較して）短時間に変化させ、活性および選択性を制御することにある。すなわち、自ら応答する自己制御型の触媒を目指す研究である。構造に柔軟性のある層状化合物は、ゼオライトなどの剛直な三次元結晶と比較すると、ホスト-ゲスト間の精密な適合性といる観点からすると一見不利のように考えられる。むしろ、この構造柔軟性を利用して自己制御型触媒を開発するのである。また、修飾剤や反応条件を制御することでこの構造柔軟性を克服し、均一構造を保持することが可能である。このような自己応答型触媒は、極めて初歩的であるが外的刺激官能部と反応活性部を組込んだ触媒としては、極めて新規性があり新しいタイプの触媒開発研究として非常に意義の高いことと考えられる。

3．　結果と考察

3．1 Interlayer Modification of Smectites with both Structural Tuning Guests and Chiral Rhodium Complexes

The catalysis of the smectite intercalated metal complexes is very sensitive to the environment of the interlayer space as described in the previous chapter. The optimization of environment reaction conducted is a key factor to achieve the high selectivity.[1,2] Although the precise control of the layer structure is required for enhancing the high selectivity, it is impossible to control the layer space by the swelling with solvents. Therefore, to control of the layer structure precisely, quaternary alkylammonium was used as a "structural tuning guest" because the alkylammonium was easily intercalated into the host by cation exchange and interlayer spacing can be changed ca. 0.13 nm per one methylene unit by varying the size of the alkylammonium employed. Furthermore, varying the length of the longitudinal chains exert the same effect as the charge density of the host.[3-5]

So far, the alkylammonium modified clay has been used in the industry as rheological controlling agents in paints, greases, and cosmetics.[6] Another application of the organo-clay to the industry is the clay-polymer nanocomposites[7-9] and the adsorbents for poorly water soluble organic species.[10,11] On the other hand, the organo-clay is the subjects in view of the molecular assemblies in the scientific field. For example, the extensive studies of the surfactant intercalated clay films have classified the highly ordered structure of the guest after various photochemical reactions, where the role of the guest surfactants is to produce the hydrophobic interlayer space, to control the state of photosensitive probes,[12-15] and to pillar organically by the accommodation of guest species.[16]

The precise structural control of the clay-intercalated catalyst by using the structural tuning guests was described in this chapter. New clay supported catalysts, in which both structural tuning guests and chiral active species were modified in the gallery of smectites, were synthesized by simple cation exchange method (Scheme 3-1). Preparation and characterization of this multiple-modified smectite (MMS) were described in the following.

Results and Discussion

Intercalation amounts of MMS

Intercalation amounts of q-C_n/smectite and MMS's are listed in Table 3-1. When q-C_{18} (0.75 equivalent of C.E.C. of NaHT) was intercalated into NaHT, intercalation amount of q-C_{18}NaHT was 0/49.4/NaHT(18). Then, Rh-DIOP$^+$ was intercalated into 0/49.4/NaHT(18) to give 7.4/41.8/NaHT(18). These intercalation amounts were expressed as 0/51.7/NaHT(18) and 8.5/48.0/NaHT(18) in % of C.E.C., respectively, indicating a part of q-C_{18} in q-C_{18}/NaHT was exchanged with Rh-DIOP$^+$ by the intercalation of Rh-DIOP$^+$ into q-C_{18}/NaHT. Similar tendency was observed in all of the MMS's as summarized in Table 3-1. These observations also suggest that no segregation be found in all of the MMS.

IR spectra for alkylammonium modified smectite and MMS

Several IR spectra for the alkylammonium modified smectites and MMS are shown in Figure 3-1 to 3-6. These assignments are summarized in Table 3-2 and 3-3. The bands at ca. 2920 cm^{-1} due to ν_{as} C-H(sp^3) and at ca. 1470 cm^{-1} due to δ C-H_2(sp^3) were assigned to the structural tuning guest. The bands at 3055 cm^{-1} due to ν C-H(sp^2) and ca. at 1435 cm^{-1} due to ν P-C(Arom) were assigned to the chiral rhodium complexes.[21,22] The bands at about 1010 and 997 cm^{-1} due to ν Si-O were assigned to the framework of the silicate layer in NaHT and LiTN, respectively.[23-25] All of the alkylammonium modified smectites showed the bands due to the host and the structural tuning guest. Then, the bands due to Rh-DIOP$^+$ were observed in all of the MMS's, and the band due to ClO_4^- as a counter anion of the rhodium complex was disappeared, clearly indicating the intercalation of the rhodium complex into alkylammonium modified smectites proceeded by cation exchange.

XRD measurements for smectites modified with structural tuning guests and MMS

XRD patterns for smectites modified with structural tuning guests and MMS are shown in from Figure 3-7 to 3-12. In all of the modified smectites, a sharp d_{001} peak of the original host shifted to the smaller angle after the intercalation of the structural tuning guest, indicating the clearance space (C.S.=d_{001}-thickness of silicate layer (0.96 nm)) was expanded to 1.85 – 2.88 nm as summarized in Table 3-4. With respect to 0/49.4/NaHT(18) and 0/36.4/NaHT(18), a shoulder peak was involved in d_{001} peak, indicating these intercalation compounds have a few phases with different interlayer

spacings. In contrast the other structural tuning guest-modified smectites a showed single phase with a sharp d_{001} peak. Then, Rh-DIOP$^+$ was intercalated into the structural tuning guest-modified smectites to give MMS. Each MMS exhibited a sharp d_{001} peak with the second and the third reflection, suggesting both Rh-DIOP$^+$ and q-C_{18} were accommodated in the same gallery without segregation. In addition the unknown phases in 0/49.4/NaHT(18) and 0/36.4/NaHT(18) were disappeared, that is, the reconstruction of the layer was occurred in the intercalation of the rhodium complex. The expansion of C.S. was observed in 10.9/54.3/NaHT(18), 7.4/41.8/NaHT(18), and 10.5/46.5/LiTN(10) after the intercalation of Rh-DIOP$^+$ into their original q-C_n/smectite. With respect to the other MMS's, their C.S. were still retained despite of the intercalation of the rhodium complex into their original q-C_n/smectite.

Kuroda et al. reported the orientation of q-C_{18} in various smectites, where the employed smectites and their C.E.C. were saponite for 70 and TSM for 120 mmol-100g clay, respectively. The intercalation amount and the basal spacing of q-C_{18}/saponite were 67 mmol-100g and 2.2 nm, respectively, and q-C_{18} formed *pseido*-trimolecular layers in the silicate sheet. In contrast those of q-C_{18}/TSM were 105 mmol-100g and 3.2 nm, respectively, and q-C_{18} formed monolayer and/or bilayer in the silicate layer.[26-28]

The difference in the orientation of the structural tuning guest between NaHT and LiTN was clearly observed. It seemed reasonable to assume that the orientation of q-C_{18} in NaHT was mono and that in LiTN was *quasi*-bilayer arrangements by the comparison of this work with their results. The tilting angle[29] of q-C_n was calculated from the C.S. and the molecular size of q-C_n, i.e. 2.76 for q-C_{18}, 2.24 for q-C_{14}, and 1.74 nm for q-C_{10}.[30,31] The tilting angles for 0/59.3/NaHT(18), 0/49.4/NaHT(18), and 0/36.4/NaHT(18) were 71, 45, and 60°, respectively, in monolayer arrangements. After the intercalation of Rh-DIOP$^+$ into q-C_{18}/NaHT, the tilting angles for 10.9/54.3/NaHT(18), 7.4/41.8/NaHT(18), and 15.4/31.4/NaHT(18) became 90, 65, and 58° in monolayer arrangements, respectively, indicating that the orientation of q-C_{18} was changed in the NaHT host.

In contrast, the tilting angle for MMS with LiTN host remained to be 90° even after the intercalation of Rh-DIOP$^+$ into q-C_n/LiTN because of its high layer charge density (about three times to NaHT). In q-C_n/LiTN each structural tuning guest formed *quasi*-bilayer ordering perpendicular to silicate layer, so that MMS showed little expansion of C.S. despite of the intercalation of the rhodium complex. Some models for MMS's with different structural tuning guests were depicted in Figure 3-13 and 3-14.

Since the orientation of Rh-DIOP$^+$ can not be detected by the characterization employed in the present work, the orientation might be regulated by the layer charge as the structural tuning guest is.

TEM photographs of the intercalation compounds

To investigate the microstructure of the intercalation compounds, TEM measurements were examined. Several photographs of smectites, q-C_{18}/smectite, and MMS are shown in Figure 3-15 to 3-20. In each photograph the fringes were regular stacking of the individual smectite layers. Uniformly expanded layers were observed in q-C_{18}/smectite and MMS, indicating the regular orientation of the structural tuning guests and Rh-DIOP$^+$. The expansion of the layer spacing in the original hosts after the intercalation was also observed in TEM photographs. The layer spacing was measured from the photographs, i.e. 0.9-1.0 for NaHT, 2.9-3.3 for 0/59.3/NaHT(18), 3.3-3.6 for 10.9/54.3/NaHT(18), 0.9-1.1 for LiTN, 2.9-3.3 for 0/46.5/LiTN(18), and 3.3-3.6 nm for

18.3/42.8/LiTN(18), respectively. These layer spacing of the intercalation compounds were a little smaller than basal spacing estimated from XRD measurements because of the removal of additional adsorbed water and/or error in measuring the layer spacing. In addition, EDS spectra of MMS showed RhL_{α_1} peak. No peak due to chlorine was detected, suggesting the intercalation proceeded by cation exchange.

Conclusion

A new type of host-guest catalyst was synthesized by a simple cation exchange in two steps under ambient atmosphere. Characterization of the intercalation compounds by FT-IR and EDS revealed that the intercalation proceeded by cation exchange. XRD and TEM measurements suggested the highly ordered structure of the intercalation compounds. The orientation of the structural tuning guests was controlled by the layer charge density of the hosts as well as the loadings of the guests. Furthermore, the structural tuning guests play important roles in the orientation control of rhodium complexes as well as the expansion of the interlayer space.

References

1. S. Shimazu, K. Ro, T. Sento, N. Ichikuni, and T. Uematsu, *J. Mol. Cat.*, **107**, 297, (1996).
2. T. Sento, S. Shimazu, N. Ichikuni, and T. Uematsu, *J. Mol. Cat.*, in press.
3. A. Weiss, *Angew. Chem.*, **75**, 113 (1963).
4. G. Lagaly, *Angew. Chem. Int. Ed. Engl.*, **15**, 575 (1976).
5. M. Ogawa and K. Kuroda, *Bull. Chem. Soc. Jpn.*, **70**, 2593 (1997).
6. T. R. Jones., *Clay Miner.*, **18**, 339 (1983).
7. B. K. G. Theng, "Formation and Properties of Clay-Polymer Complexes," Elsevier, Amsterdam (1979).
8. E. Ruitz-Hitzky, *Adv. Mater.*, **5**, 334 (1993).
9. E. P. Giannelis, *Adv. Mater.*, **8**, 29 (1996).
10. R. M, Barrer, "Zeolites and Clay Minerals as Sorbents and Molecular Sieves," Academic Press, London (1978).
11. R. M. Barrer, *Philos. Trans. R. Soc. London, Ser. A*, **311**, 333 (1984).
12. T. Seki and K. Ichimura, *Macromolecules*, **23**, 31 (1990).
13. H. Tomita and T. Itoh, *J. Chem. Soc., Chem. Commun.*,**1991**, 532.
14. K. Takagi, K. Kurematsu, and Y. Sawaki, *J. Chem. Soc., Perkin Trans. 2*, **1991**, 1517.
15. M. Ogawa, H. Kimura, K. Kuroda and C. Kato, *Clay Sci.*, **10**, 57 (1996).
16. M. Ogawa, T. Handa, K. Kuroda, C. Kato, and T. Tani, *J. Phys. Chem.*, **96**, 8116 (1992).
17. T. Kunitake, Y. Okahata, K. Tamaki, F. Kumamaru, and M. Takayanagi, *Chem. Lett.*, **1977**, 387.
18. T. Kunitake and Y. Okahata, *J. Am. Chem. Soc.*, **99**, 3860 (1977).
19. H. Favre and G. Lagaly, *Clay Miner.*, **26**, 19 (1991).
20. G. Ruehlicke and E. E. Kohler, *Clay Miner.*, **16**, 305 (1981).
21. L. J. Bellamy, "The Infra-red Spectra of Complex Molecules," Wiley, New York (1958), p. 321.
22. R. B. Harvery and J. E. Mayhood, *Can. J. Chem.*, **33**, 1552 (1955).
23. J.-R. Butruille, L. J. Michot, O. Barres, and T. J. Pinnavaia, *J. Catal*, **139**, 664 (1993).

24. H. V. Olphen and J. J. Fripiat, "Data Handbook for Clay Minerals and other Non-Metallic Materials," Pergamon Press, London (1979).
25. R. Nyquist and R. Kagel, "Infrared Spectra of Inorganic Compounds (3800 -45 cm^{-1})," Academic Press, New York (1971).
26. M. Ogawa, T. Wada, and K. Kuroda, *Langmuir*, **11**, 4598, (1995).
27. M. Ogawa, H. Shiraki, K. Kuroda, and C. Kato, *Clays Clay Miner.*, **40**, 485, (1992).
28. M. Ogawa, T. Aono, K. Kuroda, and C. Kato, *Langmuir*, **9**, 1529, (1993).
29. The tilting angle is defined as the elevation angle of the longitudinal straight chain of *q*-C_{18} to the layer plane. *cf.* G. Alberti and U. Costantino, in "Intercalation Chemistry," ed by M. S. Whittingham and A. J. Jacobson, Academic Press, New York (1982), p.147.
30. K. Okuyama, Y. Soboi, N. Iijima, K. Hirabayashi, T. Kunitake, and T. Kajiyama, *Bull. Chem. Soc. Jpn.*, **61**, 1485 (1988).
31. K. Okuyama, N. Iijima, K. Hirabayashi, T. Kunitake, and M. Kusunoki, *Bull. Chem. Soc. Jpn.*, **61**, 2337 (1988).

3. 2 Catalysis of Multiple-Modified Smectite

The optimization of the reaction field in catalytic reactions is a serious subject to achieve high activity and selectivity.[1] When certain active species are placed in various pores in inorganic crystallines, the active species will exhibit the characteristic behavior in comparison with the original active species alone. There have been extensive studies on the inorganic host-guest system in which unusual property was observed compared to the original guest.[2-7] For instance, characteristic recognitions by zeolites[8-12] and clay[13-16] have been known as shape selectivity. These characteristic recognitions are originated from constrained guest conformation, well ordered array of the guest, and interaction between host and guest.

The multiple-modified smectites characterized in the previous chapter were applied to asymmetric and stereo selective hydrogenation to give characteristic recognition. A drastic change in catalysis was observed by varying the host, that is, the drastic enhancement in the activity and selectivity was achieved by the orientation control of structural tuning guests. In this chapter the effect of the guest orientation on catalysis was studied, and the importance of the optimization in the reaction field, such as the suitable interlayer modification, was emphasized.

Results and Discussion

Catalysis of MMS with NaHT host

(1*R*)-(+)-α-pinene was hydrogenated to yield (1*R*)-(+)-*endo* and *exo*-pinane as shown in Scheme 4-1.[17-19] The catalytic performance for the homogeneous catalyst, Rh-DIOP$^+$ intercalated into NaHT (27.6/0/NaHT) and LiTN(10.2/0/LiTN), and all of the MMS was summarized in Table 4-1 and 4-2, where the selectivity is defined as selectivity (*exo*) = 100 × (*exo-endo*)/(*exo+endo*). Although Rh-DIOP$^+$ and 27.6/0/NaHT gave high selectivity, i.e. 89.6 and 84.5 %, respectively, the latter catalyst showed lower conversion at 606 kPa (28.0 %). On the other hand, 7.4/41.8/NaHT(18) showed much lower conversion (1.6 %) and moderate selectivity (52.0 %) at 606 kPa. Although the activity and selectivity were expected to rise up as increasing PH_2,[20] no distinct enhancement in the activity and selectivity was observed. Similar behavior was observed in 15.4/31.4/NaHT(18) and 10.9/54.3/NaHT(18) as shown in Figure 4-1. Their low activities may arise from the guest orientation that provide insufficient space around Rh-DIOP$^+$ in the gallery.

Catalysis of MMS depending on the orientation of structural tuning guest

To achieve excellent catalysis MMS with the highly ordered guests were required. Since LiTN has a high charge density (about three times to NaHT) the guest orientation in the gallery will take the highly ordered structure in comparison with that in NaHT host. When MMS with LiTN host was utilized to the catalytic reaction, drastic enhancement in the activity was observed. (see Table 4-2.) At 1010 kPa the conversion by 18.3/42.8/LiTN(18) was about 10-60 times higher than that for MMS with NaHT host. In addition at 202 kPa the conversion by 18.3/42.8/LiTN(18) was comparable to that by 27.6/0/NaHT at 606 kPa. The drastic enhancement originated from the difference in the guest orientation between NaHT and LiTN host. While the tilting angles of the structural tuning guests in NaHT hosts were 58 and 60° except for 10.9/54.3/NaHT(18), the angle for 18.3/42.8/LiTN(18) was 90°. Since the alkyl tuning guests in LiTN were arrayed vertically to the silicate layer due to higher layer charge density, the orientation of Rh-DIOP$^+$ in LiTN layer was assumed to be more regulated than in NaHT layer, that is, LiTN may provide the substrate the opportunity to access the active sites in the gallery, so that the high activity was observed. Consequently, the selectivity was also enhanced in LiTN host as shown in Table 4-3 and Figure 4-2. In contrast, without the structural tuning guests, such as 27.6/0/NaHT and 10.2/0/LiTN, no noticeable enhancement both in the activity and selectivity was observed.

With respect to 10.9/54.3/NaHT(18) the activity was much lower than 18.3/42.8/LiTN(18) despite of its vertical tilting angle of q-C_{18}. But 10.9/54.3/NaHT (18) is the most active among MMS with NaHT host because of its higher orientation of q-C_{18} than that of the other MMS with NaHT host. The difference in the activity between 18.3/42.8/LiTN(18) and 10.9/54.3/NaHT(18) could be hardly explained by the tilting angle. The difference was supposed to be the space around Rh-DIOP$^+$ for the reaction and/or changes in the electron density of the rhodium complexes by the layer charge.

PH_2 dependence on catalysis of MMS with LiTN host

The PH_2 dependence in catalysis was also observed in both 18.3/42.8/LiTN (18) and Rh-DIOP$^+$. (see Figure 4-3.) The PH_2 change may cause the change of the reaction pathway and also the stability of the Rh-DIOP$^+$-substrate adducts. The mechanistic scheme for Rh-DIOP$^+$ and MMS-catalyzed hydrogenation of α-pinene depending on PH_2 is shown in Figure 4-4. It is assumed that the hydrogenation *via* β-pinene (terminal olefin), which is isomerized from α-pinene, proceeded to yield the lower selectivity under lower PH_2 owing to less stable Rh-DIOP$^+$-β-pinene adduct. In contrast, the direct hydrogenation from α-pinene proceeded more to give the higher selectivity under higher PH_2, since the corresponding adduct of α-pinene (internal olefin) was sterically more favorable.

In Rh-DIOP$^+$ the selectivity and the conversion increased with increasing PH_2 until 1010 kPa, indicating the direct hydrogenation pathway from α-pinene increased. Above 1010 kPa of PH_2 the strong coordination of the hydride might elongate the Rh-P bond, so that the C_2 symmetry of the rhodium-chelated phosphine and the ligand-substrate interaction decreased. The subsequent lowering of the C_2 symmetry of the chiral phosphine ligand made the selectivity and conversion decreased, although the rhodium complexes catalyzed the direct hydrogenation of the substrate. In addition the stretch of the Rh-P bond caused the elimination of the ligand from the metal center and the subsequent aggregation of the metal species, so that the selectivity and activity decreased.

In contrast the selectivity and the conversion for 18.3/42.8/LiTN(18) kept rising even when PH_2 exceeded 1010 kPa. This catalysis in the MMS was ascribed to the retention of the well-defined chiral structure of the rhodium complexes as well as the increase of the pathway of the direct hydrogenation with increasing PH_2. The rhodium complexes in the gallery interacted with both the structural tuning guests and the silicate sheet of the host, so that the well-defined chiral structure of the original rhodium complexes was prevented from the stretch of the Rh-P bond by the strong coordination of the hydride. (see Figure 4-5.) The well-defined chiral structure of the rhodium complexes in the gallery gave the high selectivity and activity. These observation indicate the stabilization of the metal complex by intercalating the complex into the layer lattice silicate.

The PH_2 dependence was also observed in 10.7/46.9/LiTN(14) and 10.5/46.5/LiTN(10) as shown in Table 4-3, but the dependence became obscure and activity was enhanced as decreasing the size of the structural tuning guest. So far, the cause of these behavior is unknown, but probably due to the difference in electron density of the rhodium complexes in the host layer and/or the conformation of longitudinal alkyl chain of the structural tuning guest.

Stereo selective hydrogenation of 4-tert-butylcyclohexanone

Characteristic recognition of MMS above mentioned was extended to the other unsaturated substrates, that is, the recognition is well reproducible. MMS catalyzed the hydrogenation of 4-*tert*-butylcyclohexanone to yield *cis*-4-*tert*-butylcyclohexanol predominantly as shown in Scheme 4-2. The conversion and selectivity (*cis*) are summarized in Table 4-4, where the selectivity is defined as selectivity (*cis*) = 100 × (*cis-trans*)/(*cis+trans*). 18.3/42.8/LiTN(18) gave comparable selectivity and higher conversion compared to MMS with NaHT host, Rh-DIOP$^+$, and the smectite intercalated Rh-DIOP$^+$ as shown in Figure 4-6, suggesting the recognition by MMS was applicable not only for prochiral olefin but also for the other unsaturated substrate.

Furthermore, the size selectivity was found in MMS with LiTN host. MMS became more active in the order of 18.3/42.8/LiTN(18) > 10.7/46.9/LiTN(14) > 10.5/46.5/LiTN(10), that is, the conversion increased as the expansion of the clearance space.(see Figure 4-7.)

Structure of MMS after catalytic reaction

18.3/42.8/LiTN(18) was characterized by XRD and FT-IR measurements after the hydrogenation of pinene. After the reaction an original sharp d_{001} peak of MMS was shifted to the larger angle and became a little broadened, indicating that the layered structure was still retained in spite of a little shrinkage of the interlayer spacing as shown in Figure 4-8. The shrinkage was estimated to be 0.12 nm, which is nearly the same with the size of a methylene unit, and after the reaction C.S. of MMS was changed to 2.76 nm and agree well with the molecular size of q-C_{18}. (see Table 4-5.) This observation suggested that the orientation of the structural tuning guest was changed from *quasi*-bilayer to monolayer without changing the vertical tilting angle. In IR-spectra the peak νP-C(Arom) due to the rhodium complexes was still retained despite of a little decrease of peak absorbance after the reaction. (see Figure 4-9 and Table 4-6.) These characterization revealed that the layered structure was still retained under the high pressure and the rhodium complexes were present in the gallery after the reactions.

Conclusion

MMS exhibited the characteristic recognition depending on the orientation of the structural

tuning guests. The size selectivity was also observed by the layer structure of MMS. The structural tuning guests play important roles in the orientation control of the rhodium complexes as well as the expansion of interlayer space. The enhancement in the catalytic activity and selectivity was accomplished by the suitable structural modification of the host-guest catalysts. MMS stabilized the metal complexes under the high pressure, and the layered structure was still retained after the reactions.

References

1. "Preparative Chemistry Using Supported Reagent," ed by P. Laszlo, Academic Press, New York (1987).
2. M. B. McBride, *Clays Clay Miner.*, **33**, 510 (1985).
3. A. Yamagishi and M. Soma, *J. Am. Chem. Soc.*, **103**, 4640 (1981).
4. A. Yamagishi, *J. Coord. Chem.*, **16**, 131 (1987).
5. R. A. DellaGuardia and J. K. Thomas, *J. Phys Chem.*, **87**, 990 (1983).
6. T. Nakamura and J. K. Thomas, *Langmuir*, **1**, 568 (1985).
7. P. K. Ghosh and A. J. Bard, *J. Phys. Chem.*, **88**, 5519 (1984).
8. N. Y. Chen, W. G. Garwood, and F. G. Dwyer, "Shape Selective Catalysis in Industrial Applications," Marcel Dekker, New York (1989).
9. P. B. Weisz, *Pure Appl. Chem.*, **52**, 2091 (1980).
10. E. D. Derouane, *Stud. Surf. Sci. Catal.*, **19**, 1 (1984).
11. P. B. Weisz, V. J. Frilette, R. W. Maatman, and E. B. Mower, J. Catal., 1, 307, (1962).
12. D. S. Santilli and S. I. Zones, *Catal. Lett.*, **7**, 383 (1990).
13. T. J. Pinnavaia, R. Raythatha, J. G. S. Lee, L. J. Halloran, and J. F. Hoffman, *J. Am. Chem. Soc.*, **101**, 6891 (1979).
14. S. Shimazu, T. Hirano, and T. Uematsu, *Appl. Catal.*, **34**, 255 (1987).
15. S. Shimazu, T. Ishida, and T. Uematsu, *J. Mol. Catal.*, **55**, 353 (1987).
16. T. Tatsumi, K. Yamamoto, H. Tajima, and H. Tominaga, *Chem. Lett.*, **1992**, 815.
17. F. R. Hartley, "Supported Metal Complexes," Reidel, Dordrecht (1985), chap. 6.
18. G. Allandrieu, G. Descotes, J. P. Praly, and J. Sabadie, *Bull. Chem. Soc. Fr.*, **1977**, 519.
19. R. H. Grubbs, E. M. Sweet, and S. Phisabut, in "Catalysis in Organic Synthesis," ed by P. N. Rylander and H. Greenfield, Academic Press, New York (1976), p. 153.
20. M. Mazzei, W. Marconi, and M. Riocci, *J. Mol. Catal.*, **9**, 381 (1980).

Table 3-1. Intercalation amounts of q-C_n/smectite and MMS [a]

Host	Structural tuning guest	q-C_n/smectite / mmol-100g [b]	Chiral metal complex	MMS / mmol-100g [b]
NaHT	q-C_{18}	0/59.3/NaHT(18)	Rh-DIOP+	10.9/54.3/NaHT(18)
		[0/99.6/NaHT(18)]		[12.6/62.7/NaHT(18)]
		0/49.4/NaHT(18)		7.4/41.8/NaHT(18)
		[0/51.7/NaHT(18)]		[8.5/48.0/NaHT(18)]
		0/36.4/NaHT(18)		15.4/31.4/NaHT(18)
		[0/42.0/NaHT(18)]		[17.8/36.3/NaHT(18)]
LiTN	q-C_{18}	0/46.6/LiTN(18)	Rh-DIOP+	18.3/42.8/LiTN(18)
		[0/17.4/LiTN(18)]		[6.8/16.8/LiTN(18)]
	q-C_{14}	0/49.2/LiTN(14)		10.7/46.9/LiTN(14)
		[0/24.6/LiTN(14)]		[4.0/17.5/LiTN(14)]
	q-C_{10}	0/54.3/LiTN(10)		10.5/46.5/LiTN(10)
		[0/24.8/LiTN(10)]		[3.9/17.3/LiTN(10)]

[a] The first and the second values indicate intercalation amounts (mmol-100g) of Rh-DIOP+ and q-C_n (n=18, 14, and 10), respectively, obtained from CHN analyses and UV-Vis measurements, and n is a number of longitudinal chain.

[b] Intercalation amounts in blackets are expressed in % of C.E.C.

Table 3-2. Absorption peaks and peak assignments of q-C_{18}/NaHT and MMS

Sample [a]	ν C-H(sp^2)	ν_{as} C-H(sp^3)	δ C-H$_2$(sp^3)	ν P-C (Arom)	ν Si-O	ClO_4^-
NaHT	-[d]	-	-	-	1011 (vs)	-
Rh-DIOP$^+$ [b]	3054(m)	2930 (m)	1481 (w)	1435 (s)	-	623 (vs)
q-C_{18} [c]	-	2918 (s)	1470 (s)	-	-	-
0/59.3/NaHT(18)	-	2918 (s)	1469 (m)	-	1011 (vs)	-
10.9/54.3/NaHT(18)	3059 (vw)	2919 (s)	1469 (m)	1438 (w)	1011 (vs)	-
0/49.4/NaHT(18)	-	2919 (s)	1469 (m)	-	1009 (vs)	-
7.4/41.8/NaHT(18)	3058 (vw)	2918 (s)	1469 (m)	1438 (w)	1010 (vs)	-
0/36.4/NaHT(18)	-	2919 (s)	1469 (m)	-	1011 (vs)	-
15.4/31.4/NaHT(18)	3058 (vw)	2919 (s)	1469 (m)	1438 (w)	1011 (vs)	-

vs=very strong, s=strong, m=medium, w=weak, vw=very weak.

[a] The first and the second values indicate intercalation amounts (mmol-100g) of Rh-DIOP$^+$ and q-C_{18}, respectively, obtained from CHN analyses and UV-Vis measurements. [b] [Rh((*S*,*S*)-DIOP)(COD)]ClO_4. [c] $(n\text{-}C_{18}H_{37})_2(CH_3)_2NBr$.

[d] Not detected.

Table 3-3. Absorption peaks and peak assignments of q-C_n/LiTN and MMS (n=18, 14, and 10)

Sample [a]	ν C-H(sp^2)	ν_{as} C-H(sp^3)	δ C-H_2(sp^3)	ν P-C (Arom)	ν Si-O	ClO_4^-
LiTN	-[f]	-	-	-	997 (vs)	-
Rh-DIOP$^+$ [b]	3054(m)	2930 (m)	1481 (w)	1435 (s)	-	623 (vs)
q-C_{18} [c]	-	2918 (s)	1470 (s)	-	-	-
q-C_{14} [d]		2921 (s)	1469 (s)	-	-	-
q-C_{10} [e]		2924 (s)	1467 (s)	-	-	-
0/46.6/LiTN(18)	-	2918 (s)	1469 (m)	-	994 (vs)	-
18.3/42.8/LiTN (18)	3059 (vw)	2918 (s)	1469 (m)	1438 (w)	994 (vs)	-
0/49.2/LiTN (14)	-	2921 (s)	1469 (m)	-	996 (vs)	-
10.7/46.9/LiTN (14)	3059 (vw)	2923 (s)	1469 (m)	1438 (w)	998 (vs)	-
0/54.3/LiTN (10)	-	2925 (s)	1468 (m)	-	996 (vs)	-
10.5/46.5/LiTN (10)	3059 (vw)	2926 (s)	1468 (m)	1438 (w)	1003 (vs)	-

vs=very strong, s=strong, m=medium, w=weak, vw=very weak.

[a] The first and the second values indicate intercalation amounts (mmol-100g) of Rh-DIOP$^+$ and q-C_n, respectively, obtained from CHN analyses and UV-Vis measurements, and n is a number of longitudinal straight chain.

[b] [Rh((*S*,*S*)-DIOP)(COD)]ClO_4. [c] $(n\text{-}C_{18}H_{37})_2(CH_3)_2NBr$. [d] $(n\text{-}C_{14}H_{29})_2(CH_3)_2NBr$. [e] $(n\text{-}C_{10}H_{21})_2(CH_3)_2NBr$.

[f] Not detected.

Table 3-4. Structural data for structural tuning guests modified smectites and MMS

Sample	2θ / degree	d_{001} / nm	C.S.[a] / nm	Tilting angle of q-C_n[b] / degree
NaHT	7.12	1.24	0.28	-[c]
27.6/0/NaHT	3.86	2.29	1.33	-[c]
0/59.3/NaHT(18)	2.45	3.60	2.64	71
10.9/54.3/NaHT(18)	2.36	3.74	2.78	90
0/49.4/NaHT(18)	2.82	3.13	2.17	45
7.4/41.8/NaHT(18)	2.50	3.53	2.57	65
0/36.4/NaHT(18)	2.56	3.45	2.49	60
15.4/31.4/NaHT(18)	2.58	3.42	2.46	58
LiTN	7.26	1.22	0.26	-[c]
10.2/0/LiTN	4.43	1.99	1.03	-[c]
0/46.6/LiTN(18)	2.30	3.84	2.88	90
18.3/42.8/LiTN(18)	2.30	3.84	2.88	90
0/49.2/LiTN(14)	2.58	3.42	2.46	90
10.7/46.9/LiTN(14)	2.60	3.40	2.44	90
0/54.3/LiTN(10)	3.14	2.81	1.85	90
10.5/46.5/LiTN(10)	3.06	2.89	1.93	90

[a] Clearance space = d_{001}-the thickness of silicate layer (0.96 nm).

[b] Elevation angle of q-C_n longitudinal straight chain to the layer plane, based on C.S. (n=10, 14, and 18)

[c] Structural tuning guest is not present.

Table 4-1. Asymmetric hydrogenation [a] of (1*R*)-(+)-α-pinene by Rh-DIOP$^+$, Rh-DIOP$^+$/NaHT, and MMS with NaHT host

Catalyst [b]	Selectivity (*exo*) [c]	Conversion / %	PH_2 / kPa
Rh-DIOP$^+$	89.6	96.7	606
	87.5	22.2	3030
27.6/0/NaHT	84.5	28.0	606
10.9/54.3/NaHT(18)	71.0	6.0	202
	72.0	9.3	606
	74.6	9.7	1010
	82.2	18.4	3030
7.4/41.8/NaHT(18)	52.0	1.6	606
	50.5	1.7	1010
	56.4	2.9	2323
15.4/31.4/NaHT(18)	56.1	3.2	1010
	69.5	7.3	3030

[a] Reaction conditions: reaction time, 24 h; solvent, 3 ml of MeOH; T = 303 K; substrate, 6.25×10^{-4} mol; substrate/catalyst = 100.

[b] The first and the second values indicate intercalated amounts of Rh-DIOP$^+$ and q-C_{18} (mmol-100g), respectively.

[c] Selectivity (*exo*) is defined as 100×(*exo-endo*)/(*exo*+*endo*).

Table4-2. Structural data and catalytic activity for MMS [a]

MMS loading amount / mmol-100g Rh-DIOP/ q-C_{18}/Host [b]	Clearance space [c] / nm	Tilting angle of q-C_{18} / degree	Conversion / %
27.6/0/NaHT(18)	1.33	-[d]	28.0 [e]
10.9/54.3/NaHT(18)	2.78	90	9.7
7.4/41.8/NaHT(18)	2.57	65	1.7
15.4/31.4/NaHT(18)	2.46	58	3.2
10.2/0/LiTN(18)	1.03	-[d]	48.5
18.3/42.8/LiTN(18)	2.88	90	97.4

[a] Reaction conditions: reaction time, 24 h; T= 303 K; PH_2=1010 kPa; solvent, 3 ml of MeOH; catalyst, 6.25×10^{-6} mol-Rh; substrate/catalyst=100.

[b] NaHT : $[Na_{0.33}]^{+0.33}[Mg_{2.67}Li_{0.33}(Si_4O_{10})F_2]^{-0.33}$.
LiTN : $[Li]^{+1}[Mg_2Li(Si_4O_{10})F_2]^{-1}$.

[c] Clearance space=d_{001}-thickness of silicate layer (0.96 nm).

[d] q-C_{18} is not present.

[e] PH_2=606 kPa. The other conditions are identical with footnote a.

Table 4-3. Asymmetric hydrogenation [a] of (1*R*)-(+)-α-pinene by Rh-DIOP$^+$, Rh-DIOP$^+$/LiTN, and MMS with LiTN host

Catalyst[b]	Selectivity (*exo*) [c]	Conversion / %	PH_2 / kPa
Rh-DIOP$^+$	89.6	96.7	606
	87.5	22.2	3030
10.2/0/LiTN	86.2	48.5	1010
18.3/42.8/LiTN(18)	80.2	25.7	202
	88.4	80.1	606
	89.6	97.4	1010
	92.0	99.8	3030
10.7/46.9/LiTN(14)	84.5	64.5	202
	89.1	99.6	606
	92.7	100.0	3030
10.5/46.5/LiTN(10)	87.8	90.6	202
	91.7	99.6	3030

[a] Reaction conditions are identical with footnote a in Table 4-1.

[b] The first and the second values indicate intercalated amounts of Rh-DIOP$^+$ and q-C_n (mmol-100g), respectively. (n=18, 14, and 10)

[c] Selectivity (*exo*) is defined as 100×(*exo-endo*)/(*exo+endo*).

Table 4-4. Hydrogenation of 4-*tert*-butylcyclohexanone by Rh-DIOP$^+$, Rh-DIOP$^+$/smectites and MMS[a]

Catalyst [b]	Selectivity (*cis*) [c] / %	Conversion / %
Rh-DIOP$^+$	98.9	94.2
27.6/0/NaHT	99.7	94.6
10.9/54.3/NaHT(18)	95.9	11.8
7.4/41.8/NaHT(18)	82.7	9.4
15.4/31.4/NaHT(18)	99.0	67.0
10.2/0/LiTN	95.9	43.0
18.3/42.8/LiTN(18)	99.6	95.1
10.7/46.9/LiTN(14)	97.9	73.7
10.5/46.5/LiTN(10)	97.4	63.0

[a] Reaction conditions: reaction time, 24 h; solvent, 3 ml of MeOH; T = 303 K; PH_2=101 k Pa; substrate, 6.25×10^{-4} mol; substrate/catalyst = 100.

[b] The first and the second values indicate intercalated amounts of Rh-DIOP$^+$ and q-C_n (mmol-100g), respectively. (n=18, 14, and 10)

[c] Selectivity is defined as 100×(*cis-trans*)/(*cis*+*trans*).

Table 4-5. Structural data for MMS before and after catalytic reaction

Sample	2θ / degree	d_{001} / nm	C.S.[a] / nm	Tilting angle of q-C_n[b] / degree
18.3/42.8/LiTN(18) [c]	2.30	3.84	2.88	90
18.3/42.8/LiTN(18) [d]	2.37	3.72	2.76	90

[a] Clearance space = d_{001}-the thickness of silicate layer (0.96 nm). [b] Elevation angle of q-C_{18} longitudinal straight chain to the layer plane, based on C.S. (n=10, 14, and 18). [c] As prepared. [d] After reaction.

Table 4-6. Absorption peaks and peak assignments of 18.3/42.8/LiTN(18) before and after catalytic reaction

Sample [a]	ν C-H(sp^2)	ν_{as} C-H(sp^3)	δ C-H_2(sp^3)	ν P-C (Arom)	ν Si-O	ClO_4^-
LiTN	-[f]	-	-	-	997(vs)	-
Rh-DIOP$^+$ [b]	3054(m)	2930(m)	1481(w)	1435(s)	-	623(vs)
q-C_{18} [c]	-	2918(s)	1470(s)	-	-	-
18.3/42.8/LiTN(18) [d]	3059(vw)	2918(s)	1469(m)	1438(w)	994(vs)	-
18.3/42.8/LiTN(18) [e]	-	2918(s)	1469(m)	1438(vw)	996(vs)	-

vs=very strong, s=strong, m=medium, w=weak, vw=very weak.

[a] The first and the second values indicate intercalation amounts (mmol-100g) of Rh-DIOP$^+$ and q-C_{18}, respectively, obtained from CHN analyses and UV-Vis measurements, and n is a number of longitudinal straight chain. [b] [Rh((*S*,*S*)-DIOP)(COD)]ClO_4. [c] (n-$C_{18}H_{37})_2(CH_3)_2NBr$.
[d] As prepared. [e] After reaction. [f] Not detected.

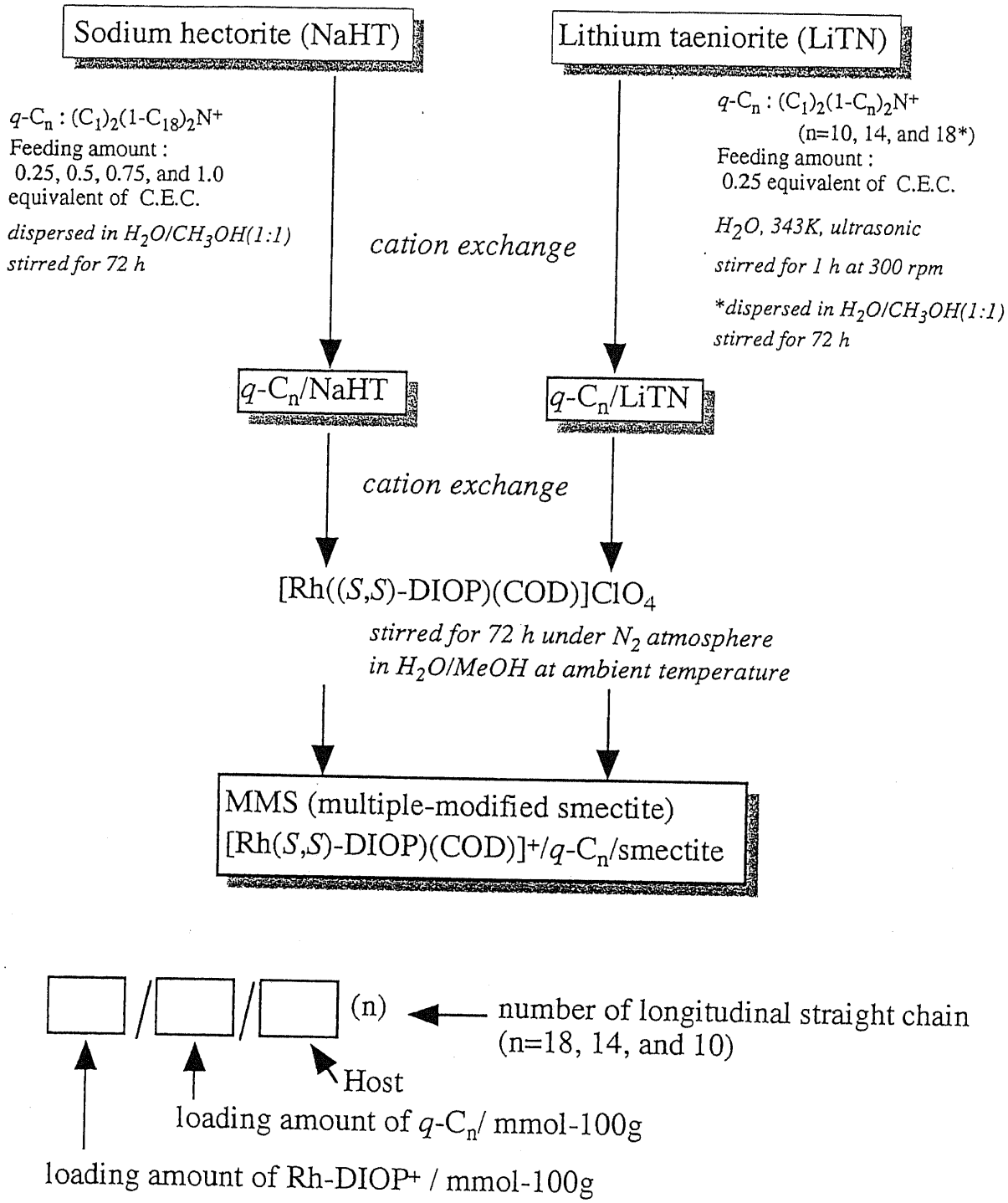

Scheme 3-1. Preparation of chiral rhodium complexes supported on structural tuning guests modified smectites (MMS).

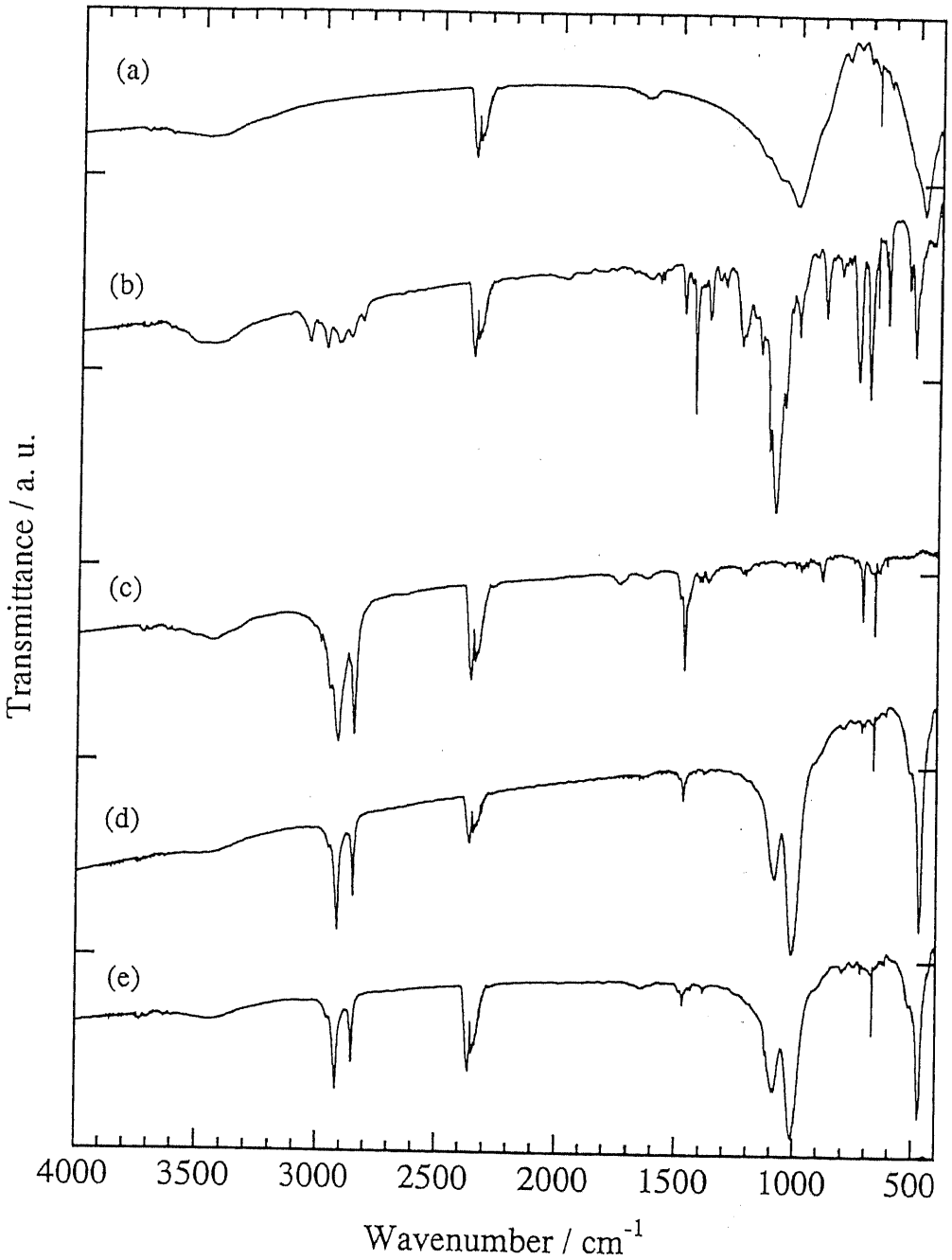

Figure 3-1. IR spectra for (a) NaHT, (b) Rh-DIOP^{+}, (c) q-C_{18}, (d) 0/59.3/NaHT(18), and (e) 10.9/54.3/NaHT(18).

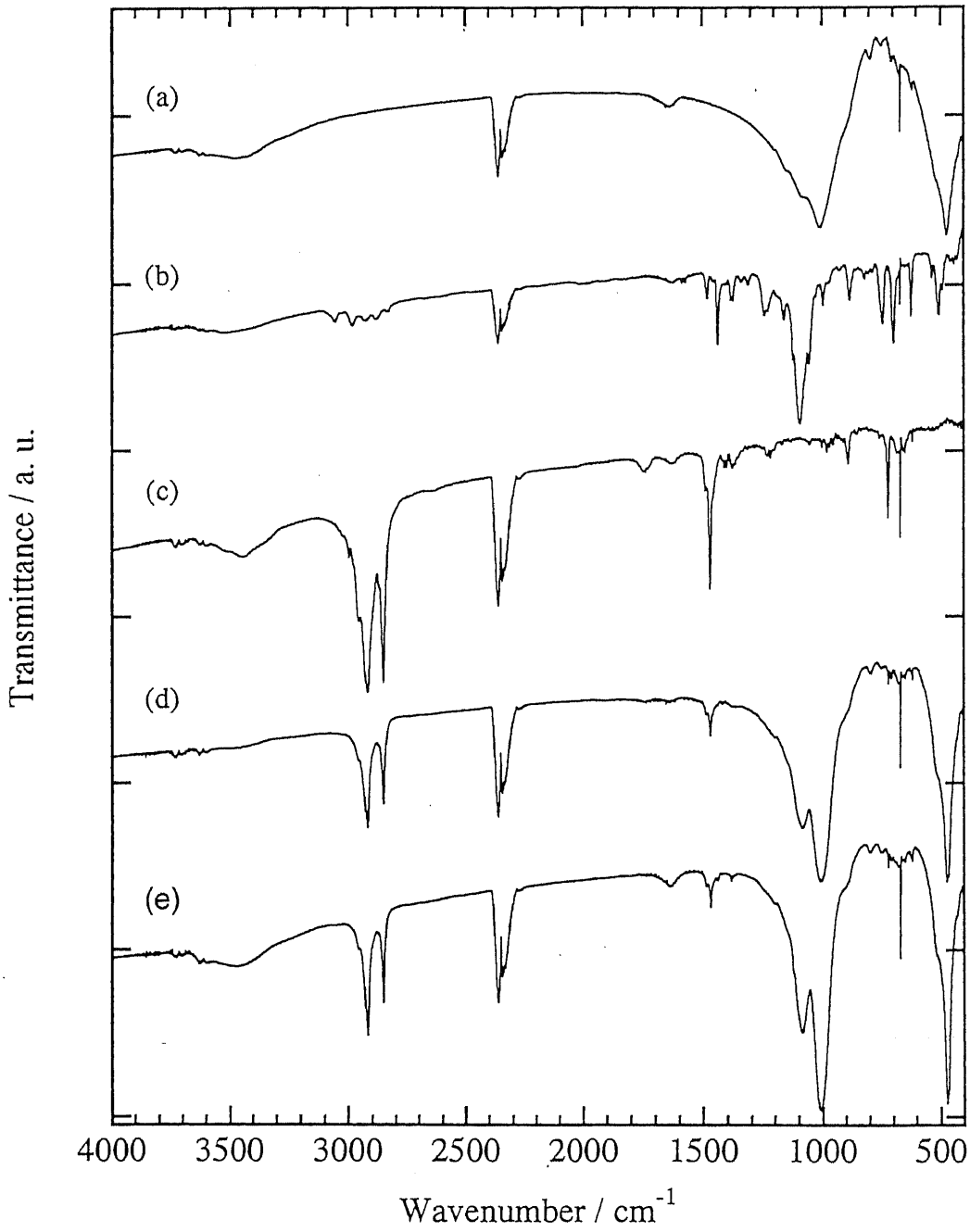

Figure 3-2. IR spectra for (a) NaHT, (b) Rh-DIOP^{+}, (c) q-C_{18}, (d) 0/49.4/NaHT(18), and (e) 7.4/41.8/NaHT(18).

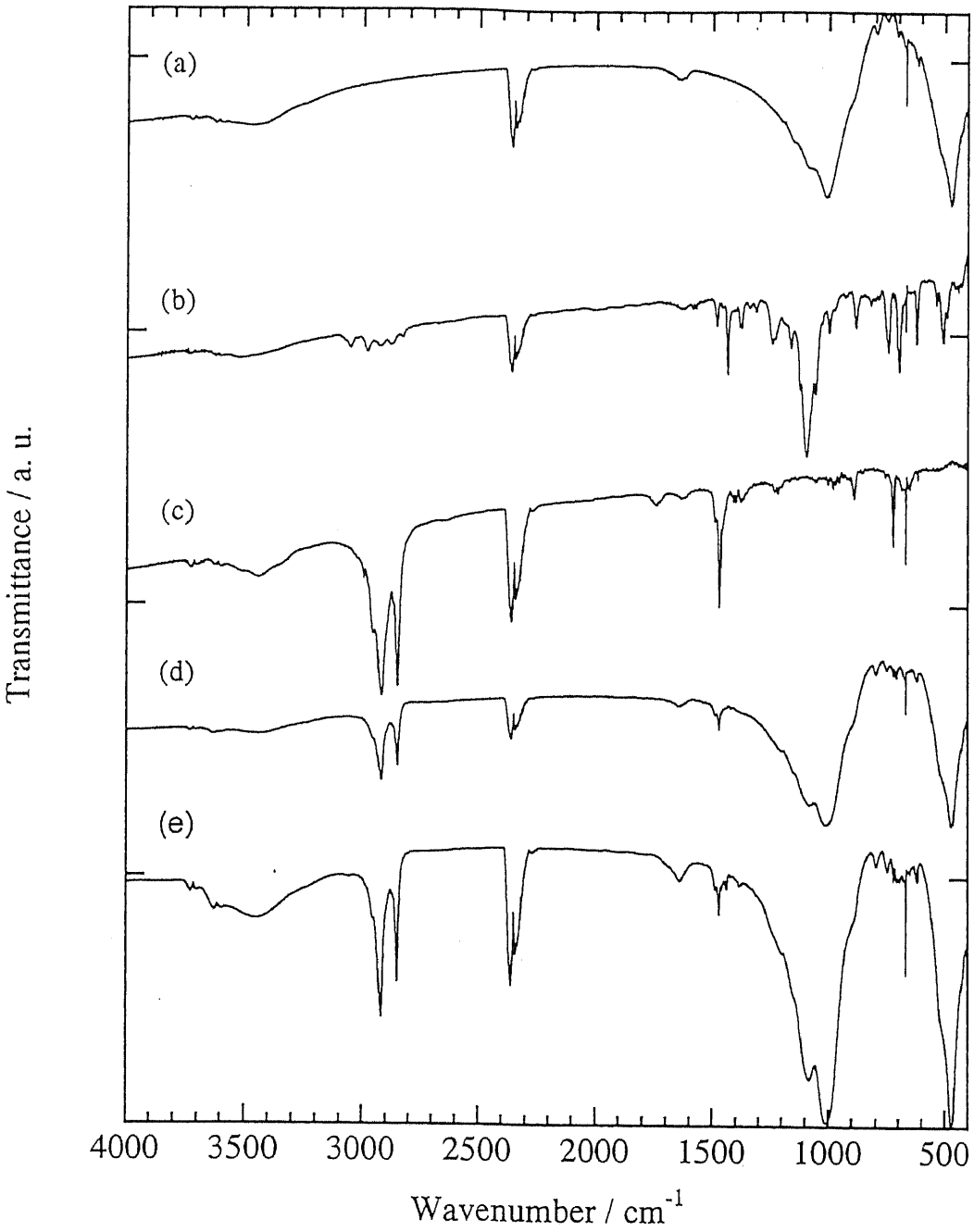

Figure 3-3. IR spectra for (a) NaHT, (b) Rh-DIOP^{+}, (c) q-C_{18}, (d) 0/36.4/NaHT(18), and (e) 15.4/31.4/NaHT(18).

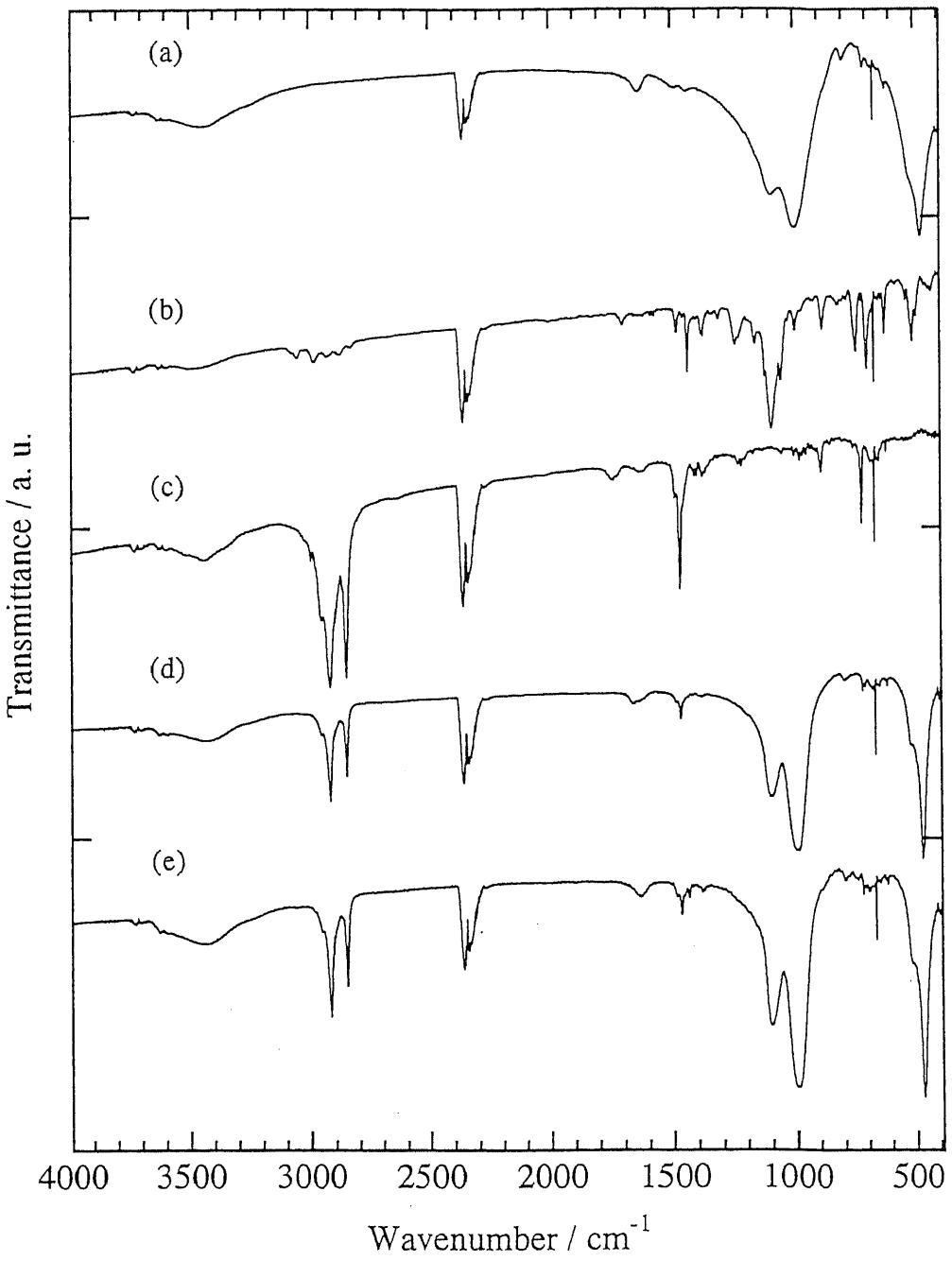

Figure 3-4. IR spectra for (a) LiTN, (b) Rh-DIOP^{+}, (c) q-C_{18}, (d) 0/46.6/LiTN(18), and (e) 18.3/42.8/LiTN(18).

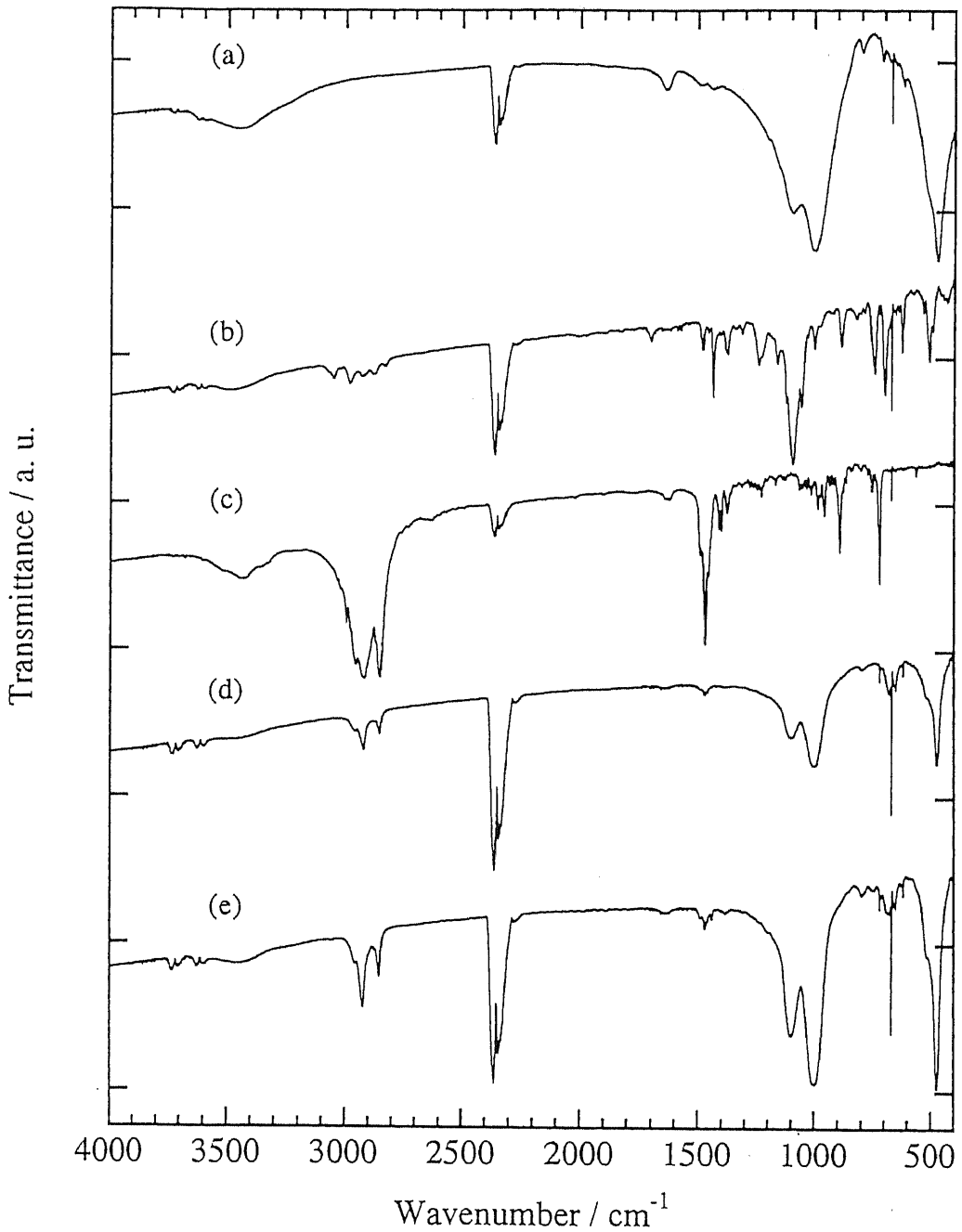

Figure 3-5. IR spectra for (a) LiTN, (b) Rh-DIOP^{+}, (c) q-C_{14}, (d) 0/49.2/LiTN(14), and (e) 10.7/46.9/LiTN(14).

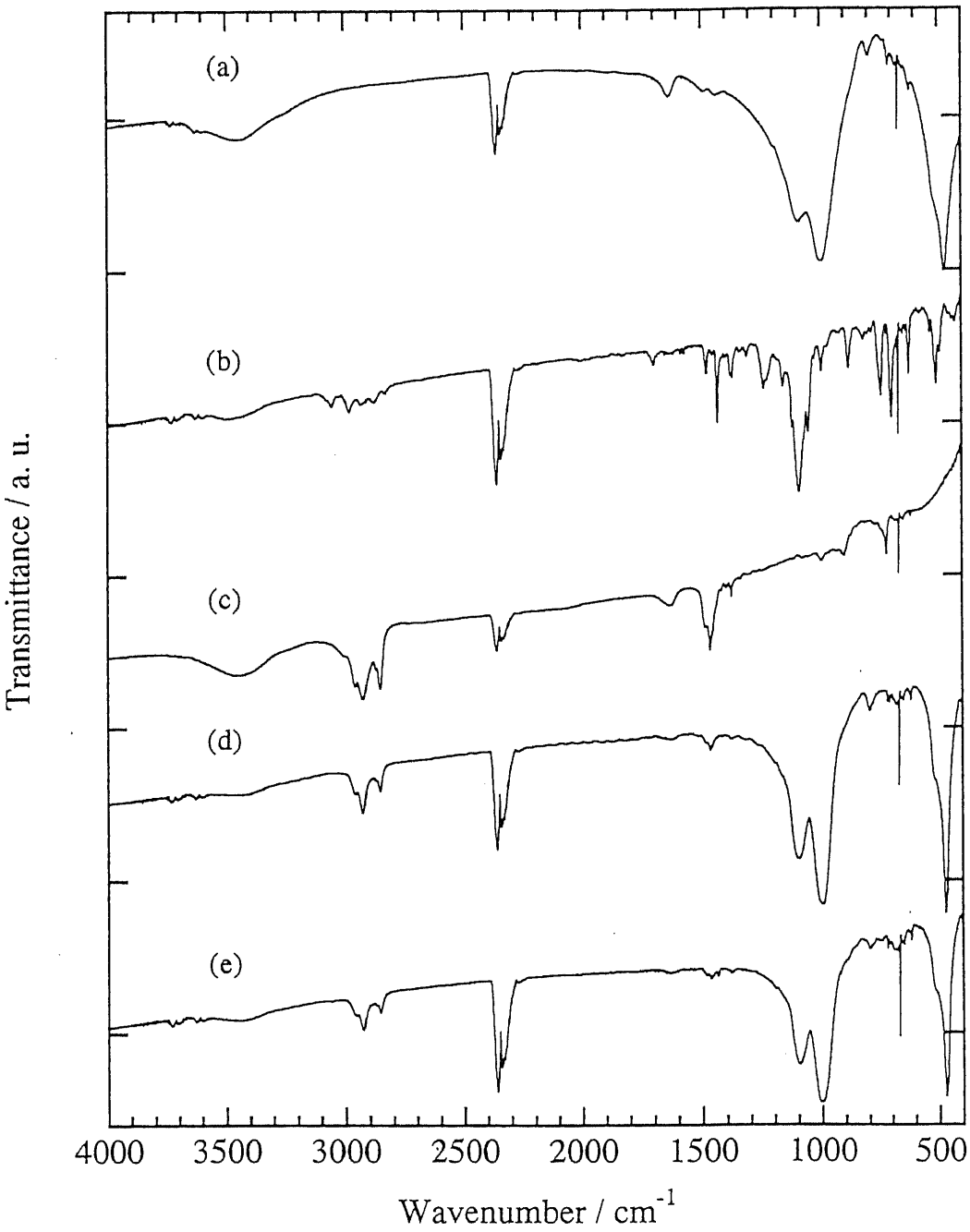

Figure 3-6. IR spectra for (a) LiTN, (b) Rh-DIOP^{+}, (c) q-C_{10}, (d) 0/54.3/LiTN(10), and (e) 10.5/46.5/LiTN(10).

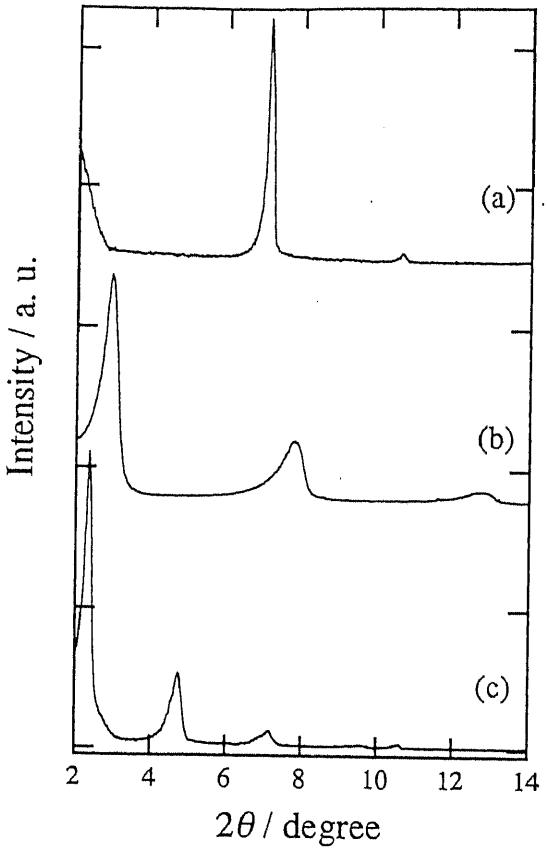

Figure 3-7. XRD patterns for (a) NaHT, (b) 0/59.3/NaHT(18), and (c) 10.9/54.3/NaHT(18).

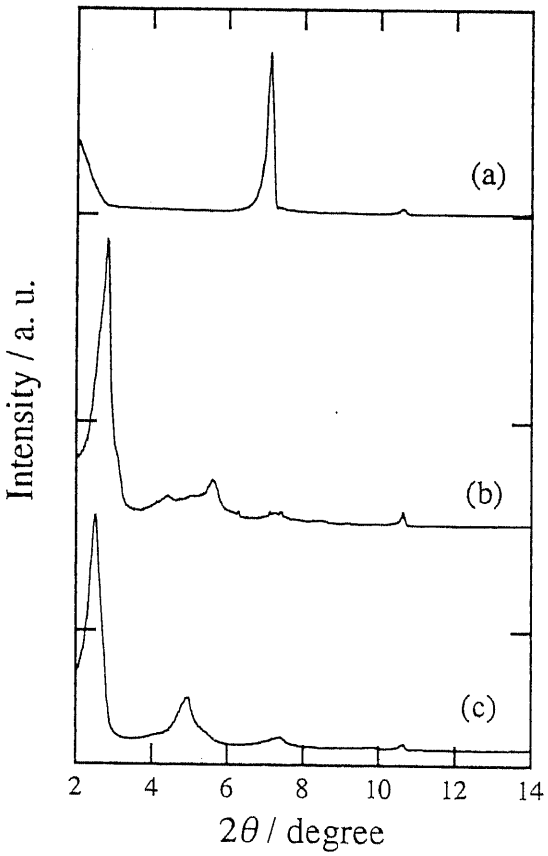

Figure 3-8. XRD patterns for (a) NaHT, (b) 0/49.4/NaHT(18), and (c) 7.4/41.8/NaHT(18).

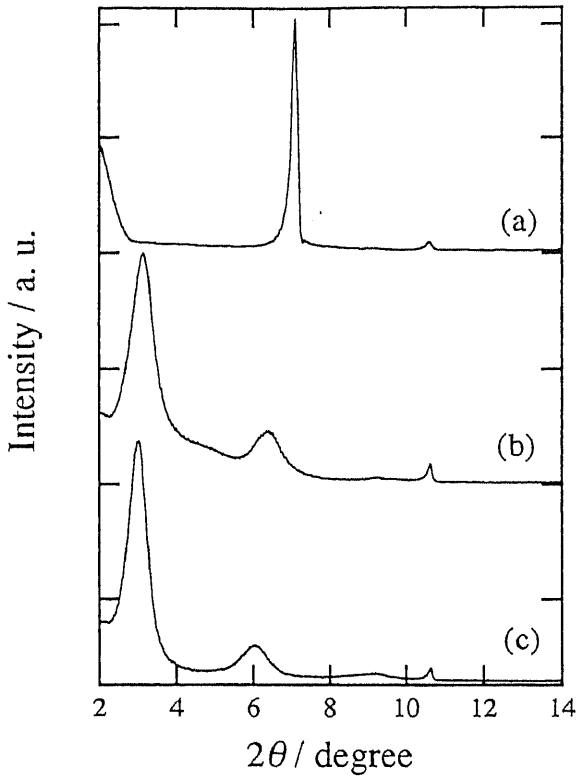

Figure 3-9. XRD patterns for (a) NaHT, (b) 0/36.4/NaHT(18), and (c) 15.4/31.4/NaHT(18)

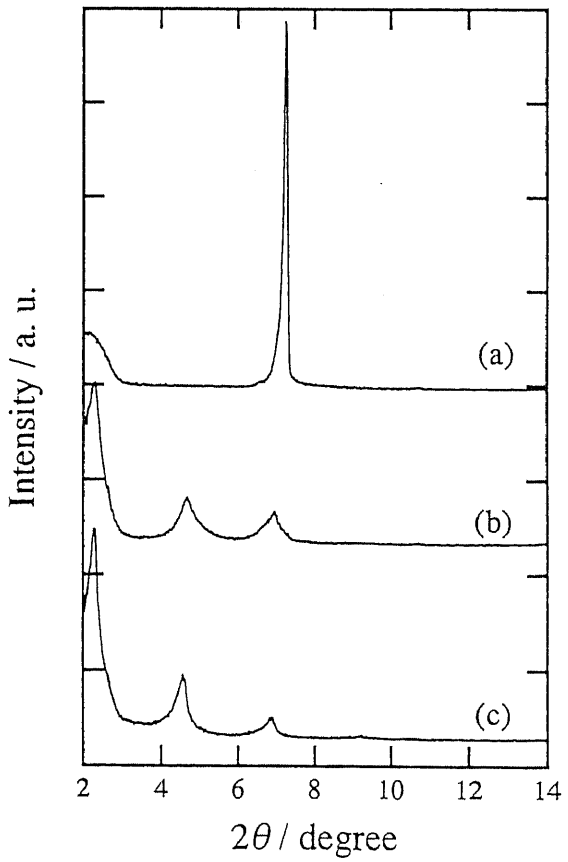

Figure 3-10. XRD patterns for (a) LiTN, (b) 0/46.6/LiTN(18), and (c) 18.3/ 42.8/LiTN(18).

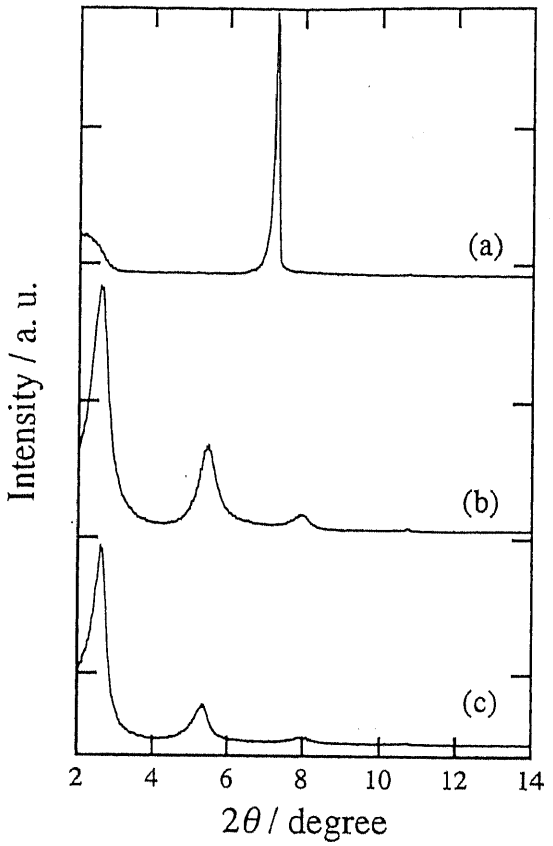

Figure 3-11. XRD patterns for (a) LiTN, (b) 0/49.2/LiTN(14), and (c) 10.7/ 46.9/LiTN(14).

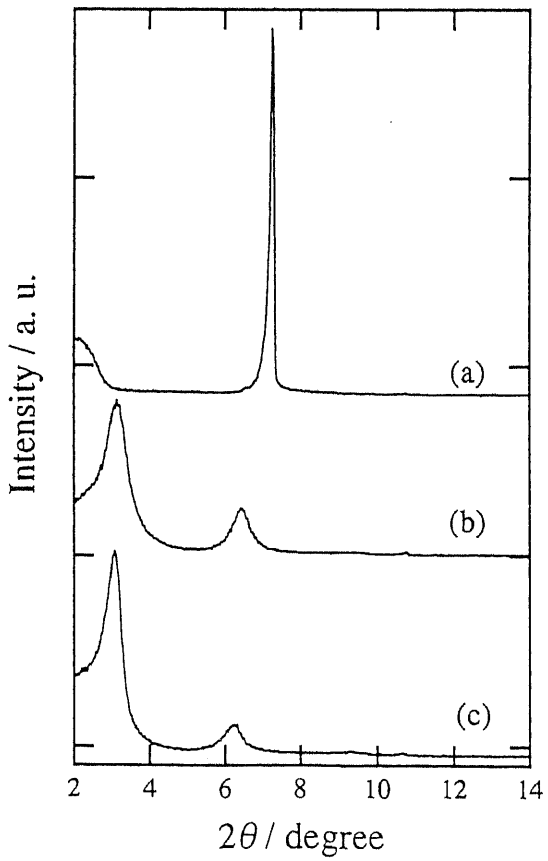

Figure 3-12. XRD patterns for (a)LiTN, (b) 0/54.3/LiTN(10), and (c) 10.5/ 46.5/LiTN(10).

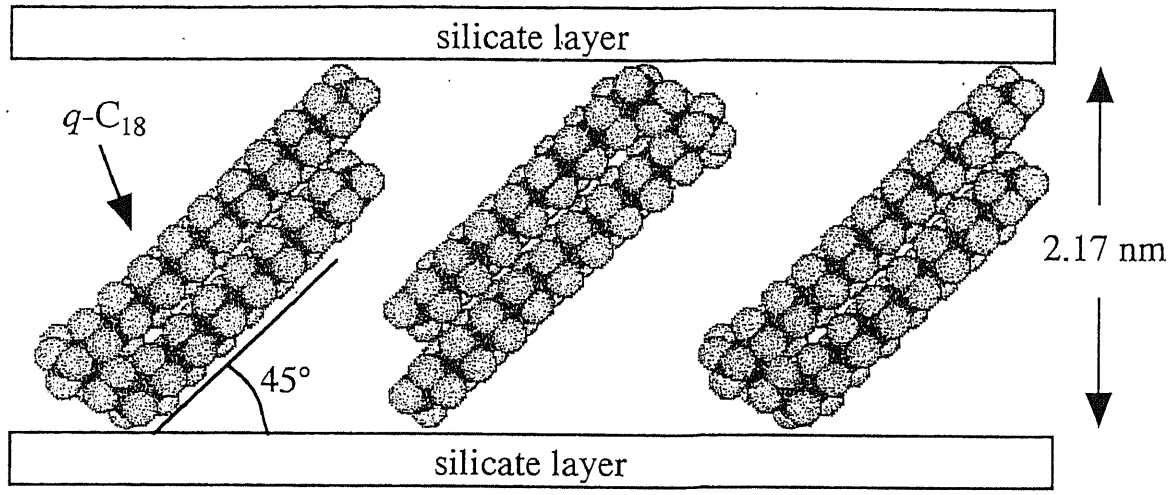

0/49.4/NaHT(18)

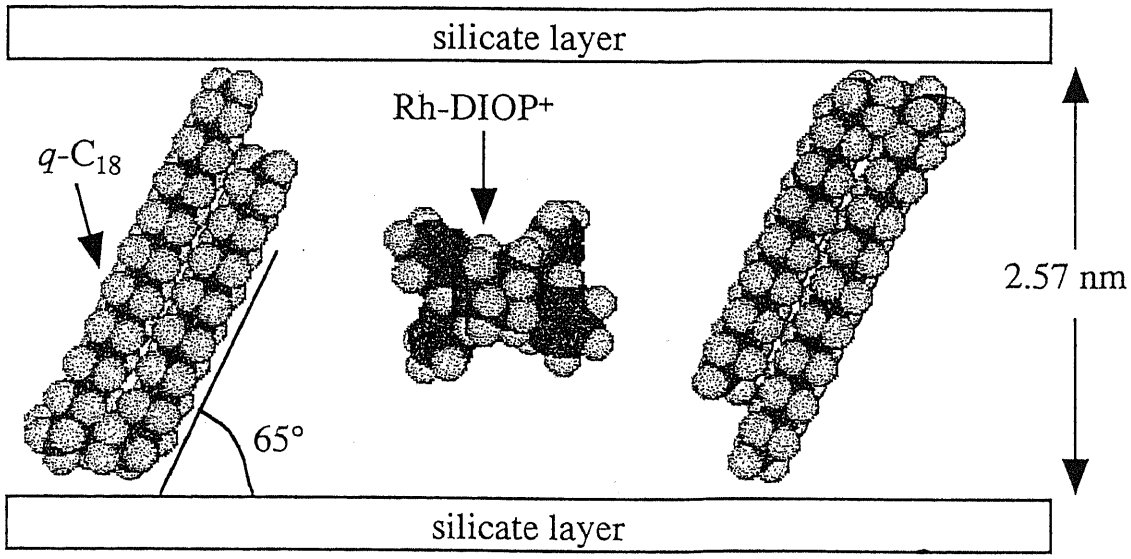

7.4/41.8/NaHT(18)

Figure 3-13. Plausible structures of 0/49.4/NaHT(18) and 7.4/41.8/NaHT(18).

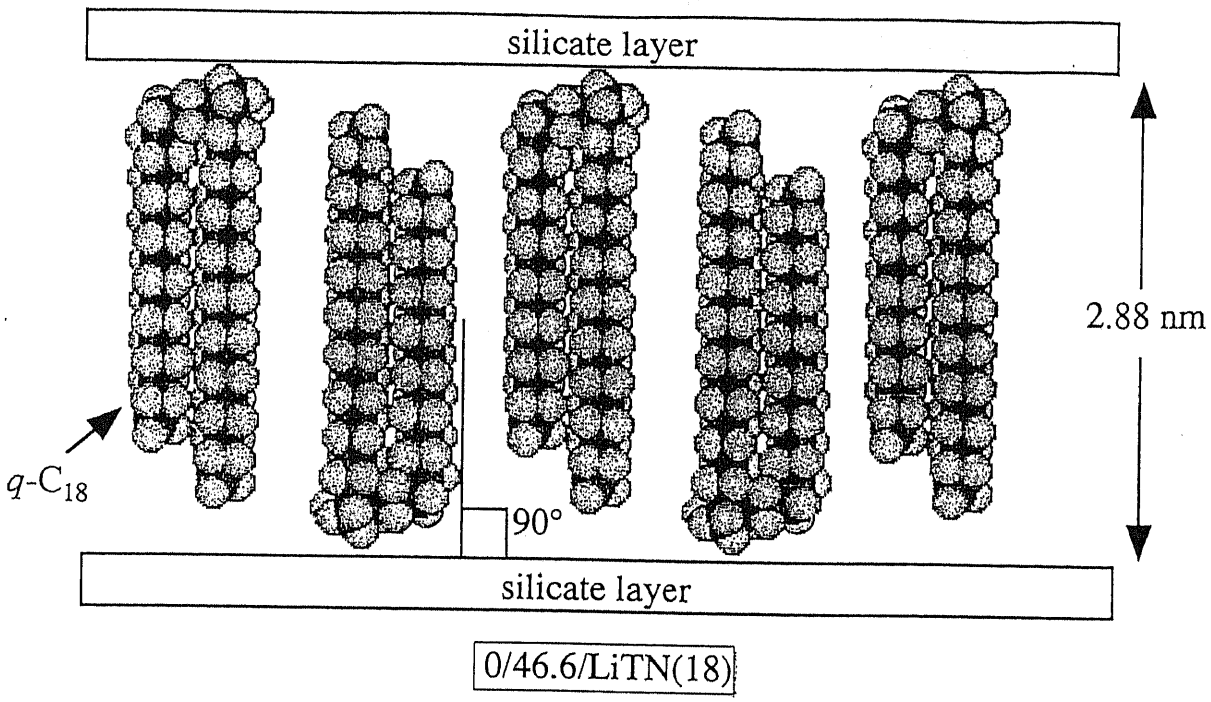

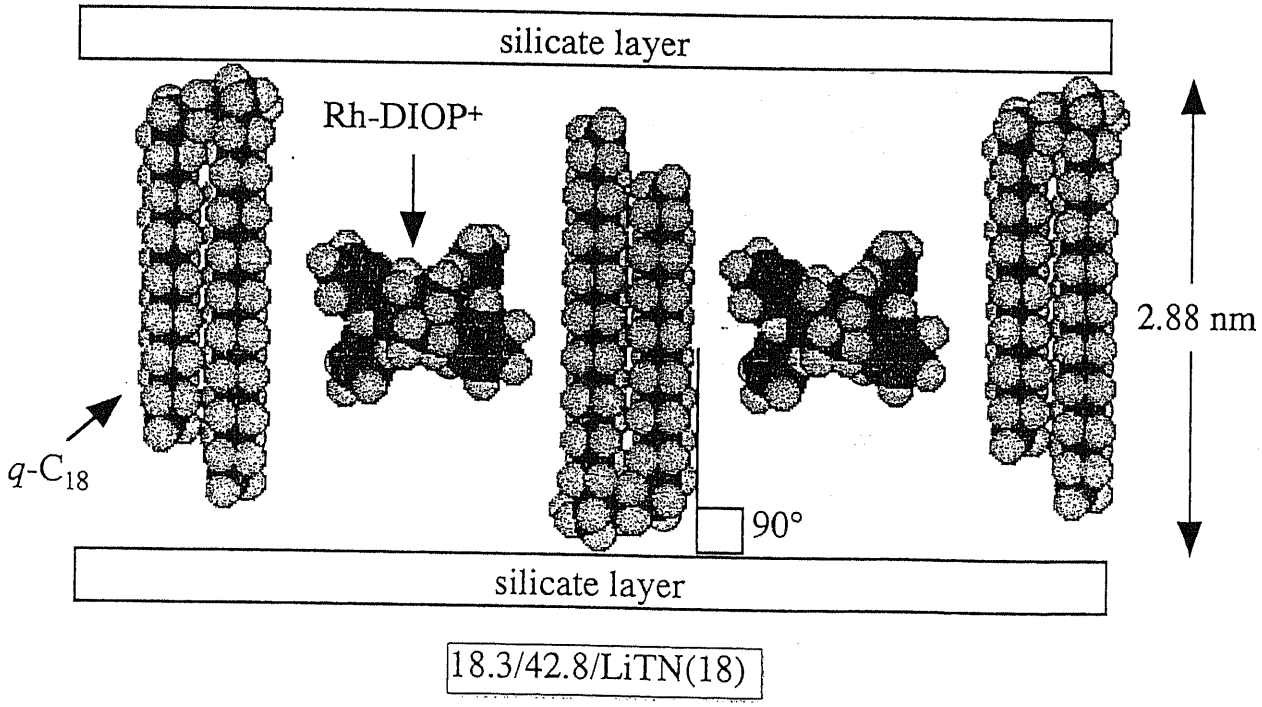

Figure 3-14. Plausible structures of 0/46.6/LiTN(18) and 18.3/42.8/LiTN(18).

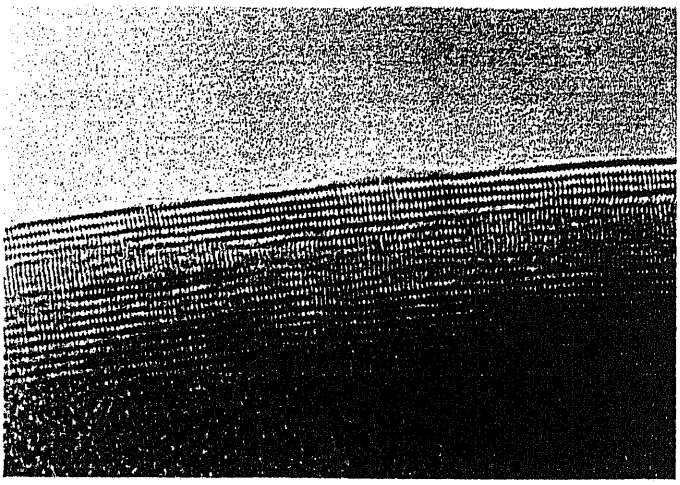

Figure 3-15. TEM photograph of NaHT.
(×400 k ×3.4)

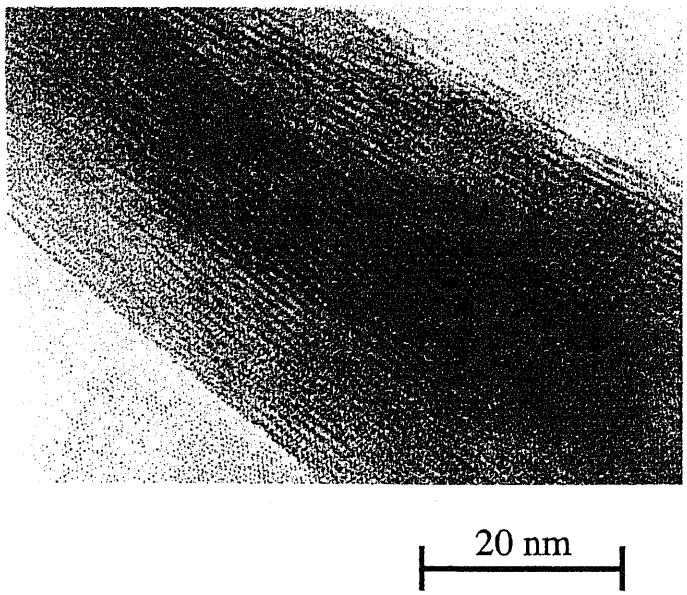

Figure 3-16. TEM photograph of LiTN.
(×400k ×3.4)

Note: Hexagonal holes on the surface of silicate layer are found in background.

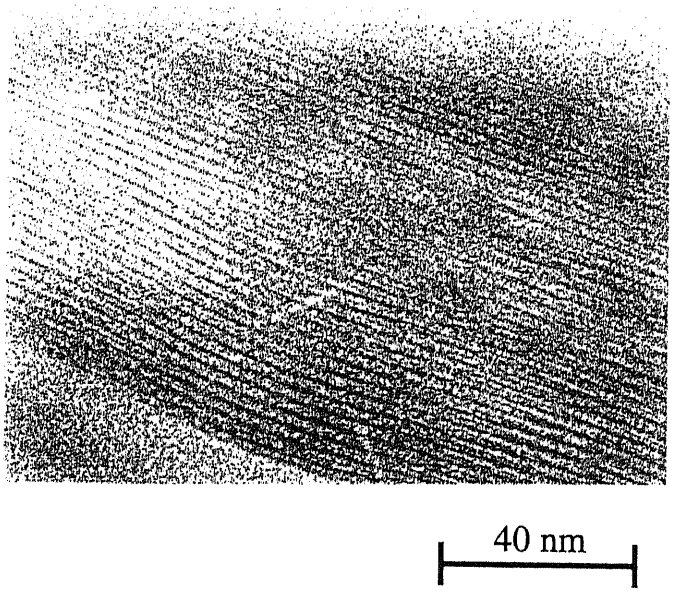

Figure 3-17. TEM photograph of 0/59.3/NaHT(18).
(×200k ×3.4)

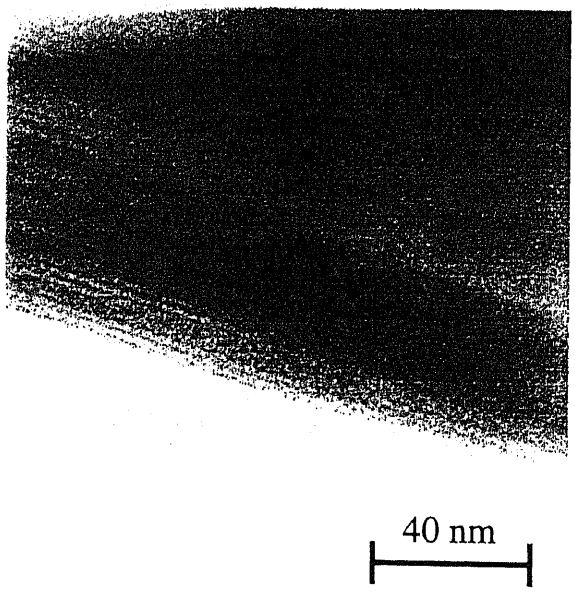

Figure 3-18. TEM photograph of 0/46.6/LiTN(18).
(×400k ×1.4)

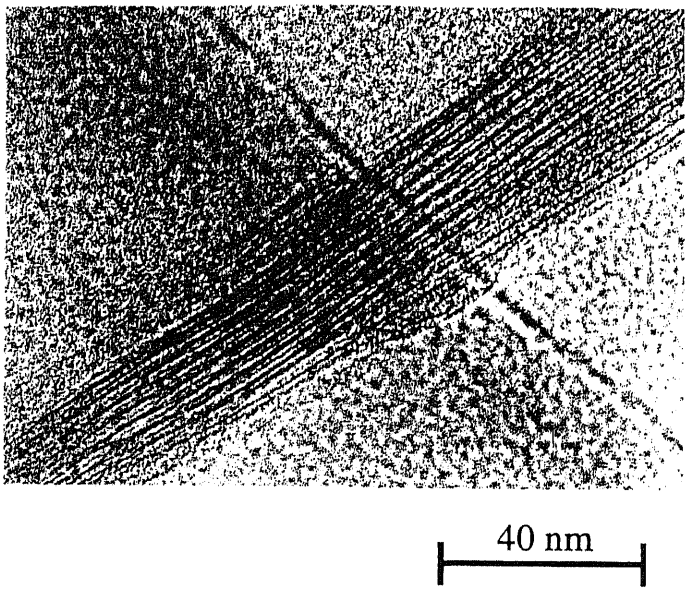

Figure 3-19. TEM photograph of 10.9/54.3/NaHT(18).
(×200k ×3.4)

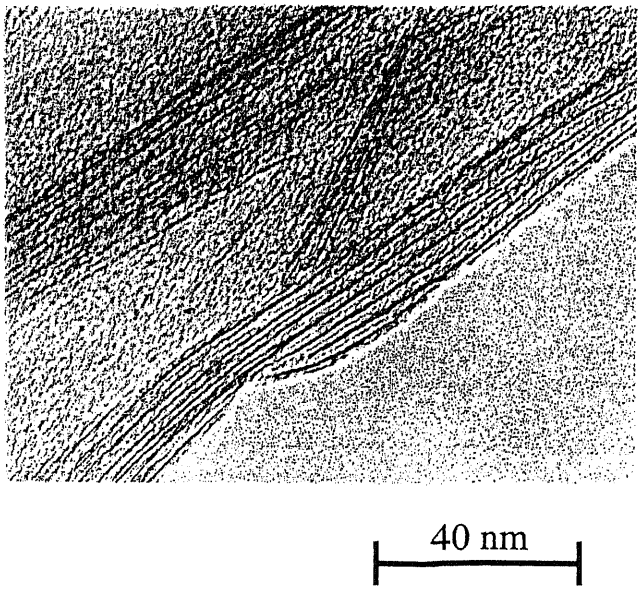

Figure 3-20. TEM photograph of 18.3/42.8/LiTN(18).
(×200k ×3.4)

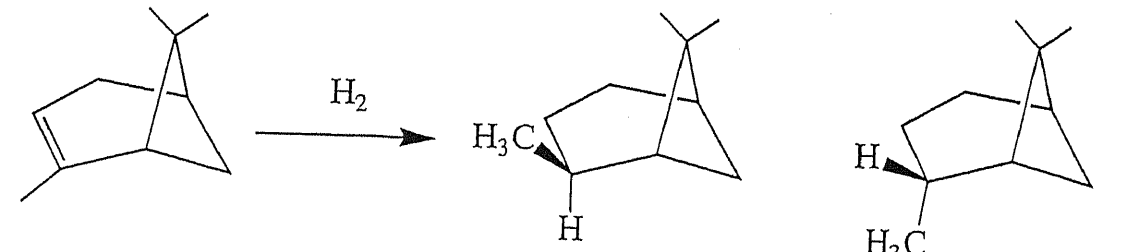

Scheme 4-1. Asymmetric hydrogenation of (1*R*)-(+)-α-pinene

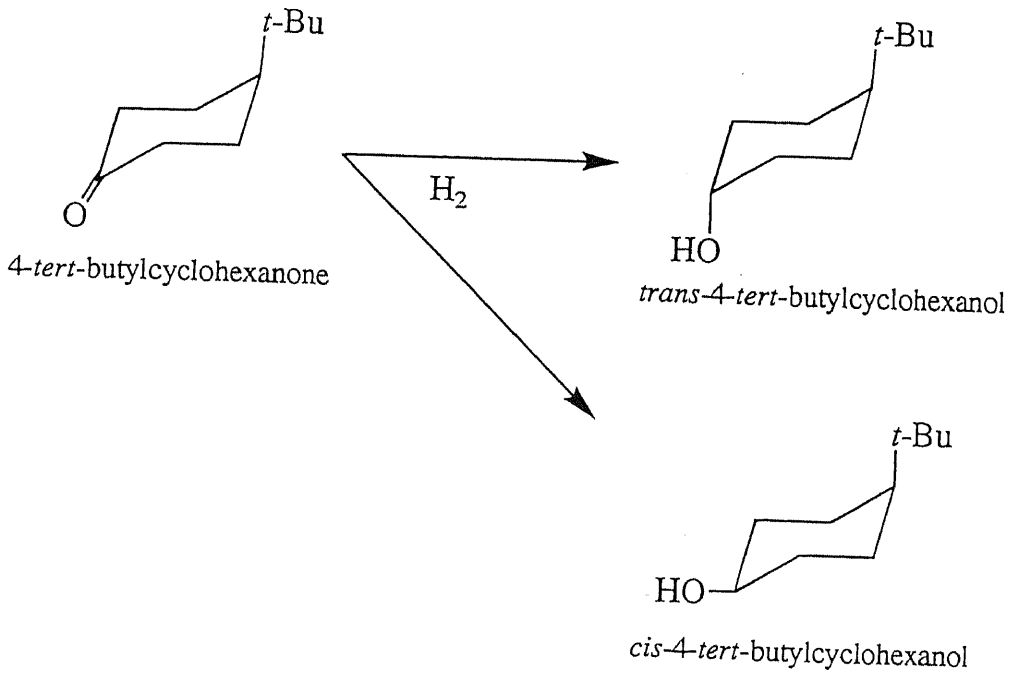

Scheme 4-2. Stereo selective hydrogenation of 4-*tert*-butylcyclohexanone

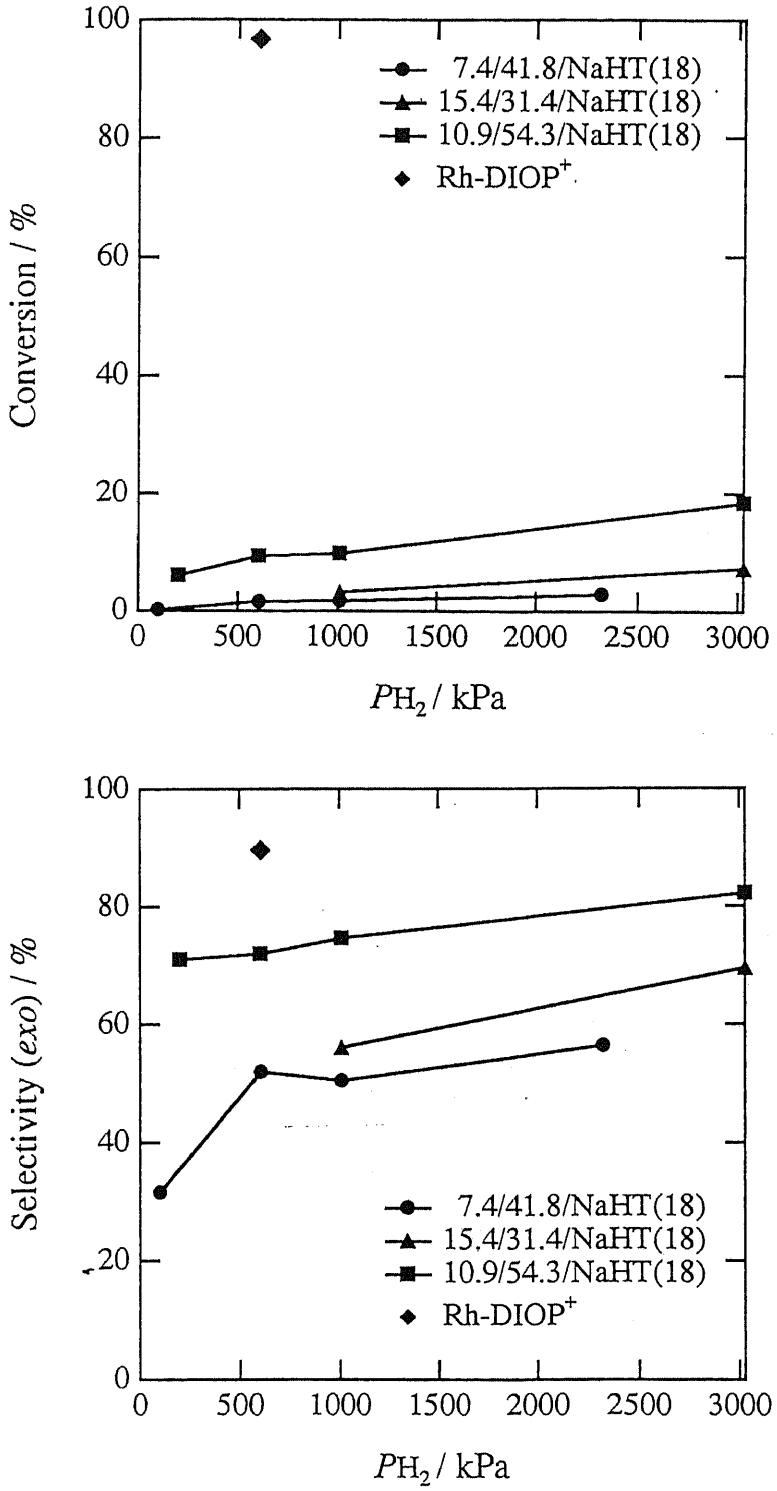

Figure 4-1. PH_2 dependence on activity and selectivity in asymmetric hydrogenation of (1*R*)-(+)-α-pinene.

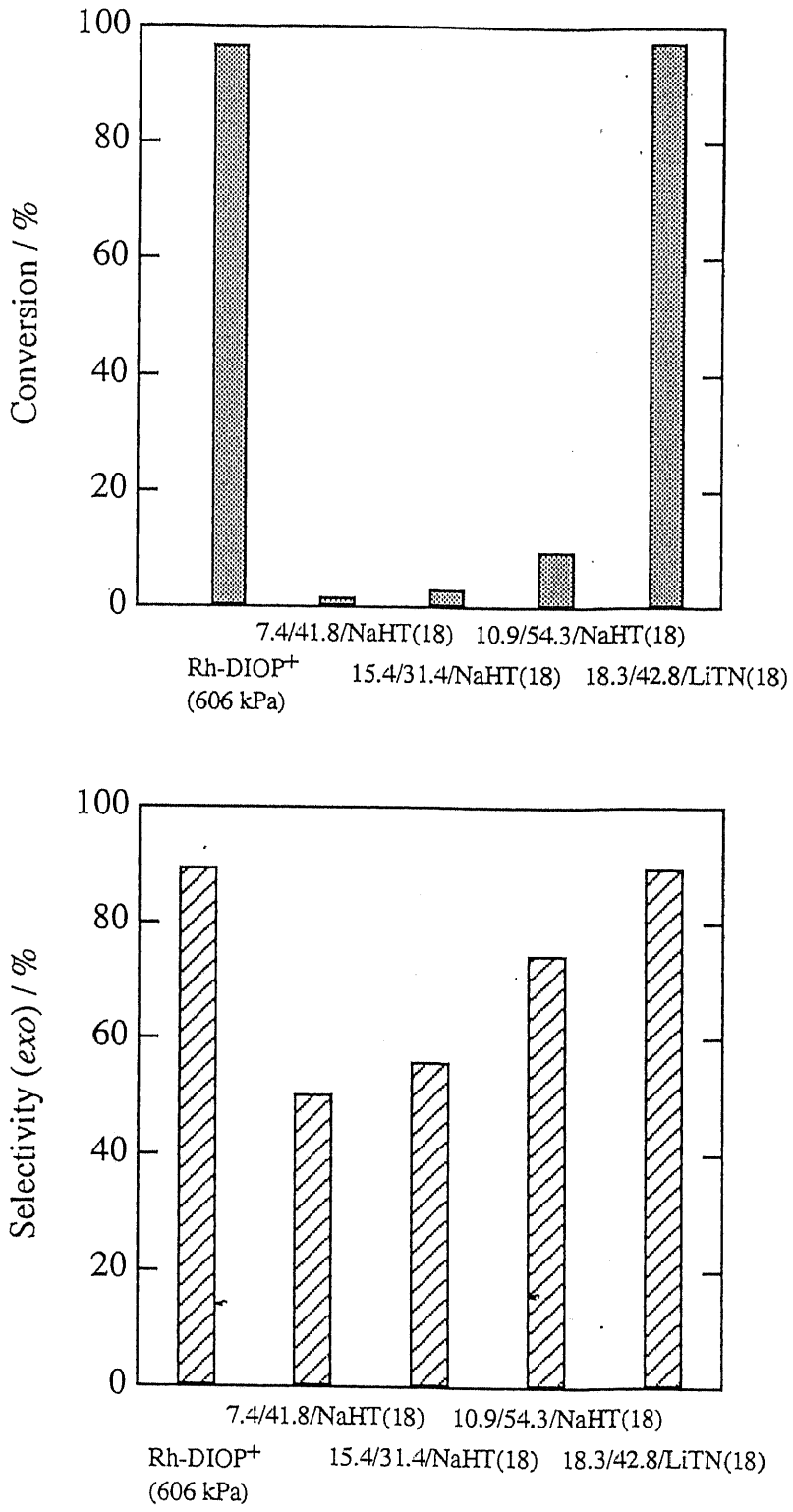

Figure 4-2. Activity and selectivity for various MMS in asymmetric hydrogenation of (1*R*)-(+)-α-pinene at 1010 kPa of H_2.

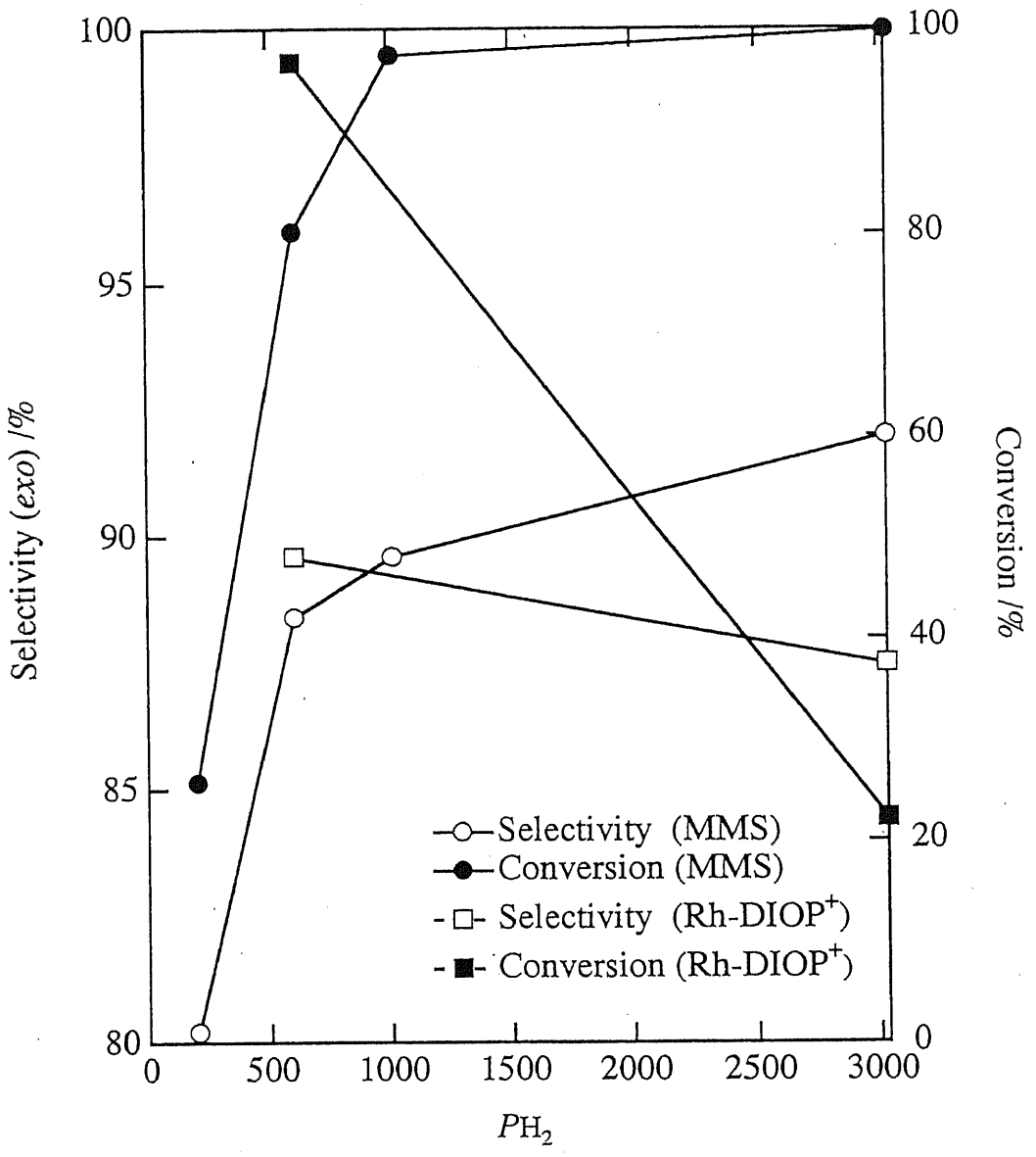

Figure 4-3. PH_2 dependence on activity and selectivity in asymmetric hydrogenation of (1*R*)-(+)-α-pinene by 18.3/42.8/LiTN(18).

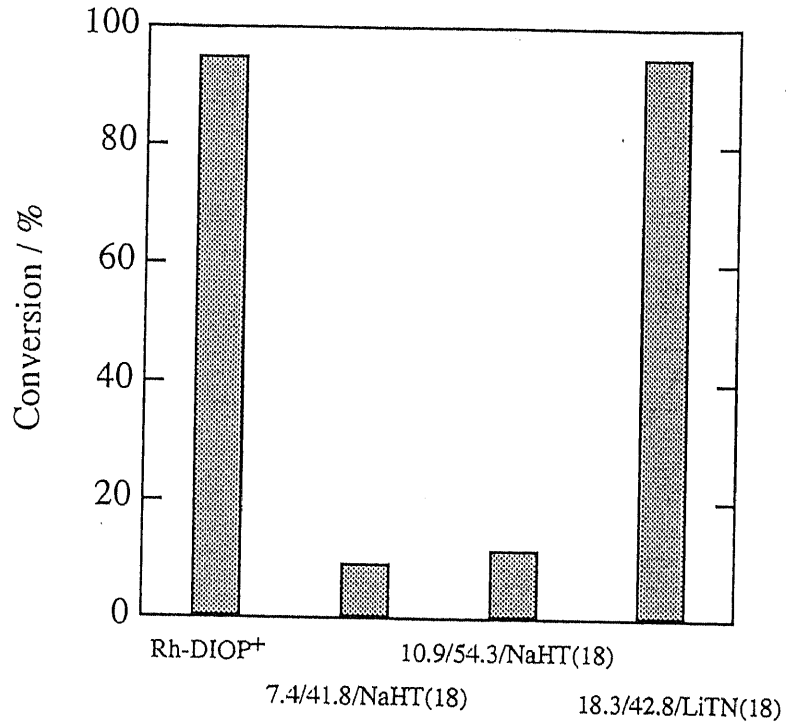

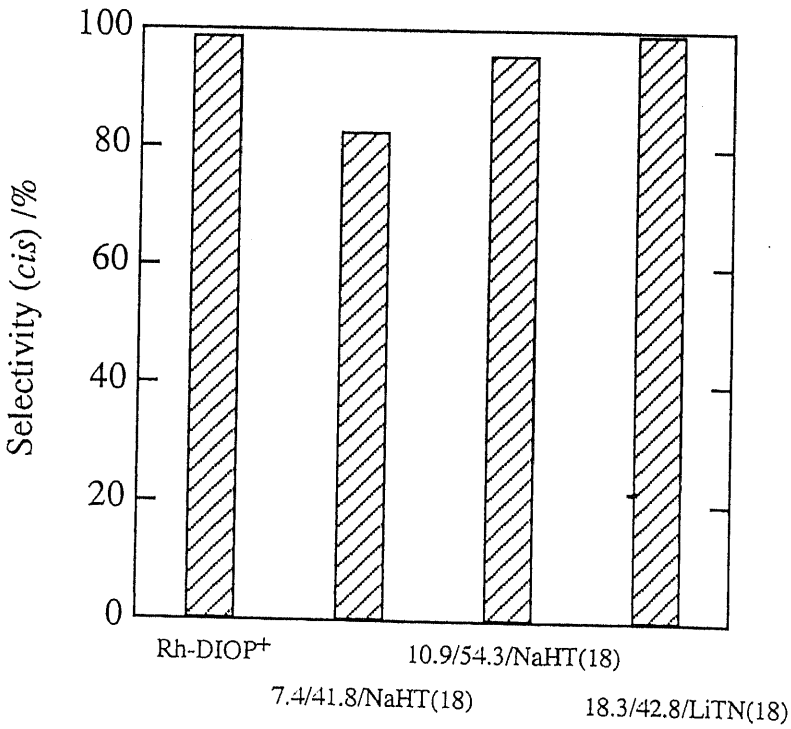

Figure 4-4. Activity and selectivity for various MMS in stereo selective hydrogenation of 4-*tert*-butylcyclohexanone.

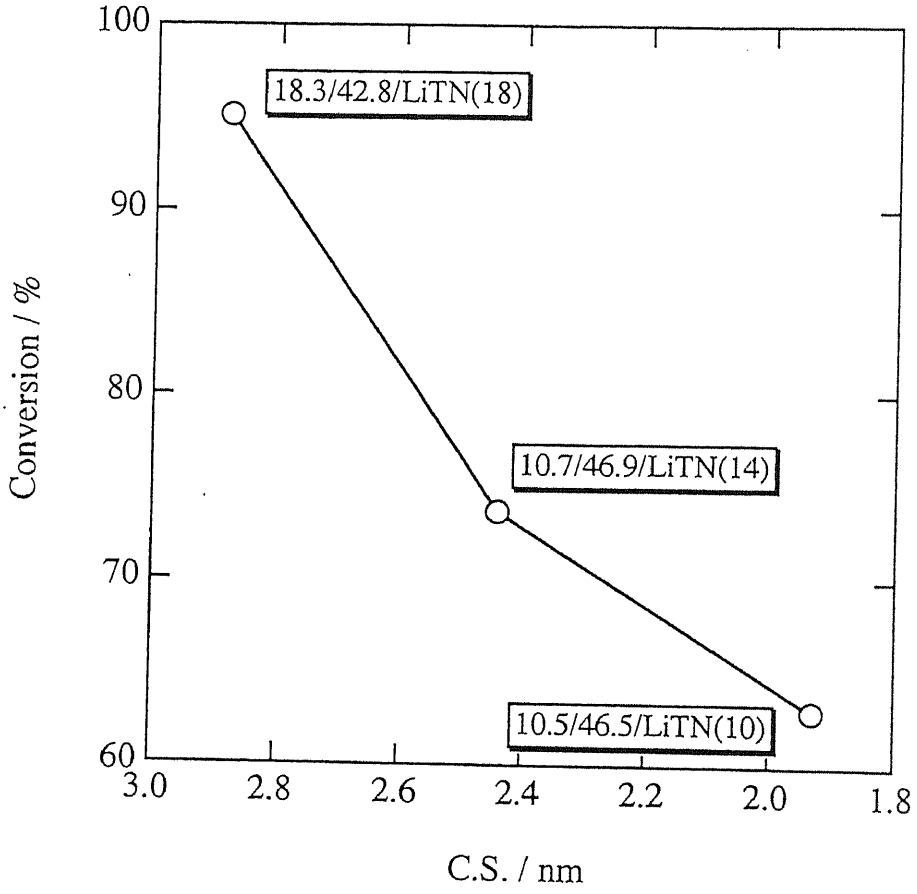

Figure 4-5. Conversion by MMS with LiTN host as a function of C.S. in stereo selective hydrogenation of 4-*tert*-butylcyclohexanone.

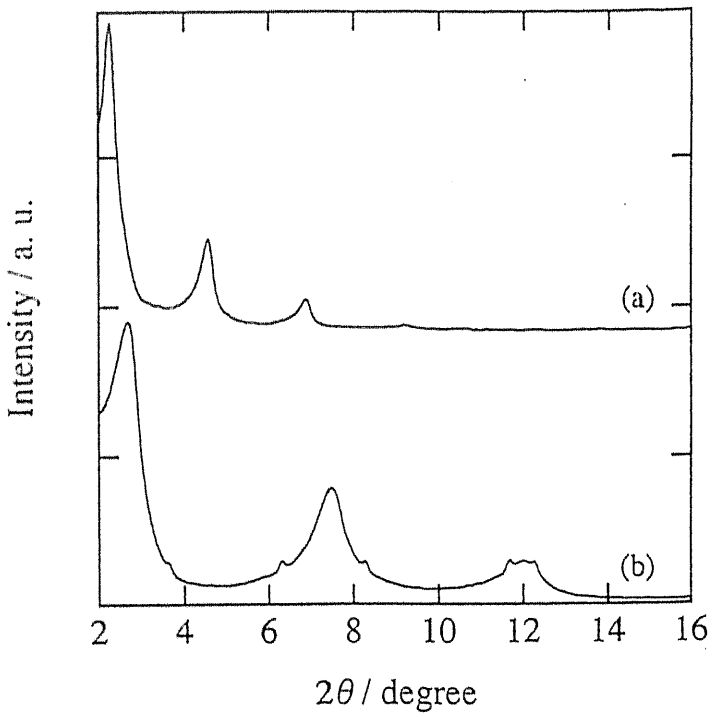

Figure 4-6. XRD patterns for (a) 18.3/42.8/LiTN(18) (as prepared) and (b) 18.3/42.8/LiTN(18) (after reaction).

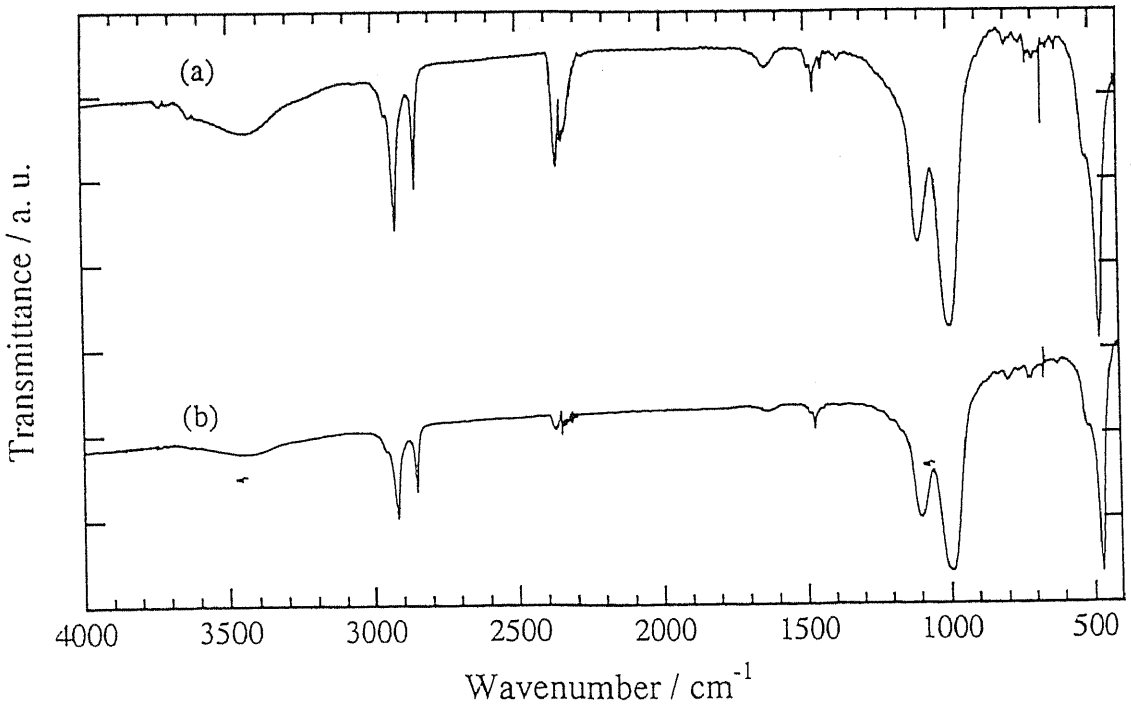

Figure 4-7. IR spectra for (a) 18.3/42.8/LiTN(18) (as prepared) and (b) 18.3/42.8/LiTN(18) (after reaction).